Non-linear Optomechanics

Nonlinearity in the restoring force of a multilayer graphene resonator

Marnix Huibers

TU Delft University of Technology
Quantum Nanoscience MED

with supervision of Vibhor Singh and Gary Steele

February 21, 2016

Contents

1 Introduction

Graphene has been attracting a lot of attention because of its special physical properties[1]. It consists of a single layer of carbon atoms producing a hexagonal atomic structure. Due to its high electron mobility (higher than $2 \cdot 10^5\ cm^2V^{-1}s^{-1}$)[2] it has potential electronic applications such as transistors[3]. Also the mechanical properties make graphene interesting. With a breaking strenght of 42 Nm^{-1} graphene is the strongest material ever measured[4]. The extraordinary electronic and mechanical properties are an important drive in the research regarding graphene.

Graphene has a very low mass density[5] and is very thin[5]. The low mass density causes large zero point motion ($x_{zpf} \propto \sqrt{1/m}$) and the low thickness leads to a large quality factor[6]. Graphene employed as a resonator has, mainly because of its low mass density and its high quality factor, attractive mechanical apllications such as mass sensing[7] and force sensing[8].

Cavityoptomechanics is a technique that involves the study of the interaction of electromagnetic radiation with mechanical systems via radiation pressure[9],[10]. It has been used to bring mechanical systems to their quantum groundstate with side band cooling[11] and to entangle microwave photons with the motion of a mechanical resonator[12]. To investigate the mechanical properties of graphene, coupling between graphene and a superconducting cavity can be made. The mechanical motion of the oscillating graphene capacitively couples to the microwave cavity. It has proven to have good position sensitivity [13]. This approach has yielded a displacement sensitivity of 17 $fm/\sqrt{Hz}$[14].

In this report coupling between a multilayer graphene oscillator and a superconducting microwave cavity is made. The production technique is described in [14]. The objectives are to determine a nonlinear term in the restoring force of the oscillating graphene and to qualitatively investigate the behavior of the oscillator. The importance of the effect of a nonlinear term in the restoring force on the motion of graphene has been recognized[15]. The internal and external dissipation rate of the microwave cavity were found to be $2\pi \cdot 51.7\ kHz$ and $2\pi \cdot 197.8\ kHz$ respectively. The resonance frequency of the cavity was $2\pi \cdot 5.901\ GHz$ and the resonance frequency of the mechanical oscillator was $2\pi \cdot 36.360\ MHz$. Measurement of the value of the quality factor yielded 148899 in the low backaction regime accompanied with a value of α of $3.3 \cdot 10^{16}\ kg/m^2s^2$. The quality factor and the value of α were 62769 and $3.2 \cdot 10^{17}\ kg/m^2s^2$ respectively in the high backaction regime. It was concluded that backaction decreases the quality factor of the mechanical resonator and increases the value of α in the restoring force.

2 Background theory

2.1 Linear Oscillator

The derivation of the amplitude and phase equations of the linear oscillator and other explanations are based on [16]. Oscillation is a periodic variation of position in time about an equilibrium point. Most oscillators can be thought of as a mass on a spring.

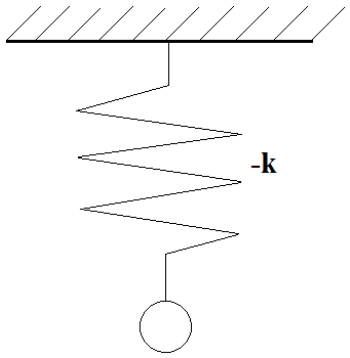

Figure 2.1: A mass on a spring oscillating around its equilibrium position.

A Taylor expansion of the potential of an oscillator around its equilibrium can be made.

$$V(x) = V(x - x_0) + \frac{dV}{dx}(x - x_0) + \frac{1}{2}\frac{d^2V}{dx^2}(x - x_0)^2 + O((x - x_0)^3) \tag{2.1}$$

At equilibrium the first derivative of the potential is zero. When terms of order $(x - x_0)^3$ and higher are neglected the potential near equilibrium is given by a parabola. The force corresponding with this potential is given by the equation below.

$$F_{restoring} = -kx \tag{2.2}$$

Equation (2.2) is called the linear restoring force (Hooke's law). The variable k reflects the stiffness of the spring. A driving force and a damping force can influence the motion of an oscillator. The assumption is made that the damping force is linear proportional to the speed at which the ossilator moves and that the driving force has a sinusoidal form.

$$F_{damping} = -l\dot{x} \qquad and \qquad F_{drive} = Bcos(\omega t) \tag{2.3}$$

The equation of motion of an oscillator is now given below.

$$m\ddot{x} = \underbrace{-kx}_{\text{restoring force}} \quad \underbrace{-l\dot{x}}_{\text{damping force}} + \underbrace{Bcos(\omega t)}_{\text{driving force}} \tag{2.4}$$

Rewriting and dividing by m gives:

$$\ddot{x} + Q^{-1}\omega_0\dot{x} + \omega_0^2 x = \omega_0^2 Acos(\omega t) \tag{2.5}$$

The relations of the symbols between equation (2.4) and equation (2.5) are given in equation (2.6).

$$Q^{-1} = \frac{l}{m\omega_0} \qquad \omega_0 = \sqrt{\frac{k}{m}} \tag{2.6}$$

Q is called the quality factor of the oscillator and the ω_0 the resonance frequency. When the motion of the oscillator is given by its steady state solution the energy loss due to damping is matched by the work done

by the driving force. A steady state pattern of oscillation is expected with the same frequency as the driving force. A solution that should be tried is given by the equation below.

$$x(t) = x_0 cos(\omega t - \phi) \tag{2.7}$$

Substituting this solution into equation (2.5) gives equation (2.8).

$$(\omega_0^2 - \omega^2)x_0 cos(\omega t - \phi) - x_0 Q^{-1}\omega_0 \omega sin(\omega t - \phi) = \omega_0^2 A cos(\omega t) \tag{2.8}$$

Equation (2.8) can be rewritten.

$$[x_0(\omega_0^2 - \omega^2)cos(\phi) + x_0 Q^{-1}\omega_0\omega sin(\phi) + \omega_0^2 A]cos(\omega t) + [x_0(\omega_0^2 - \omega^2)sin(\phi) - x_0 Q^{-1}\omega_0\omega = cos(\phi)]sin(\omega t) = 0 \tag{2.9}$$

This leads to a system of two equations.

$$x_0(\omega_0^2 - \omega^2)cos(\phi) + x_0 Q^{-1}\omega_0\omega sin(\phi) + \omega_0^2 A = 0 \tag{2.10a}$$

$$(\omega_0^2 - \omega^2)sin(\phi) - Q^{-1}\omega_0\omega cos(\phi) = 0 \tag{2.10b}$$

The solution of this system is shown below.

$$x_0 = \frac{\omega_0^2 A}{[(\omega_0^2 - \omega^2)^2 + Q^{-2}\omega_0^2\omega^2]^{\frac{1}{2}}} \tag{2.11a}$$

$$\phi = \arctan\left(\frac{Q^{-1}\omega_0\omega}{\omega_0^2 - \omega^2}\right) \tag{2.11b}$$

Substituting the calculated values into equation (2.7) gives:

$$x(t) = \frac{\omega_0^2 A}{[(\omega_0^2 - \omega^2)^2 + Q^{-2}\omega_0^2\omega^2]^{\frac{1}{2}}} \cos\left[\omega t - \arctan\left(\frac{Q^{-1}\omega_0\omega}{\omega_0^2 - \omega^2}\right)\right] \tag{2.12}$$

The left image in figure 2.2 shows a plot of the dimensionless amplitude of the oscillation for different values of Q. It is clear from the figure that a higher value of the quality factor, which means less damping, leads to a larger amplitude. The amplitude is maximal when the driving force is at the resonance frequency of the oscillator ($\omega = \omega_0$). The right image shows the phase difference between the driving force and the motion of the oscillator. For driving frequencies far below the resonance frequency the response of the oscillator tends to be in phase with the external drive. For driving frequencies far above the resonance frequency the response of the oscillator tends to be in anti-phase with the drive. For higher quality factors the transition from in phase to out of phase gets sharper. The amplitude of the linear oscillator (equation (2.11a)) is often approximated with the help of a Taylor series of the square root in the denominator and $\omega \approx \omega_0$. Using this approach the expression below is obtained for the amplitude of the linear oscillator.

$$x_0 = \frac{A}{Q^{-1} + \left(\frac{\omega - \omega_0}{Q^{-1/2}\omega}\right)^2} \tag{2.13}$$

The shape of this curve is called a Lorentzian. A plot of the dimensionless amplitude for different values of Q is shown. Note that the amplitude function is now symmetric.

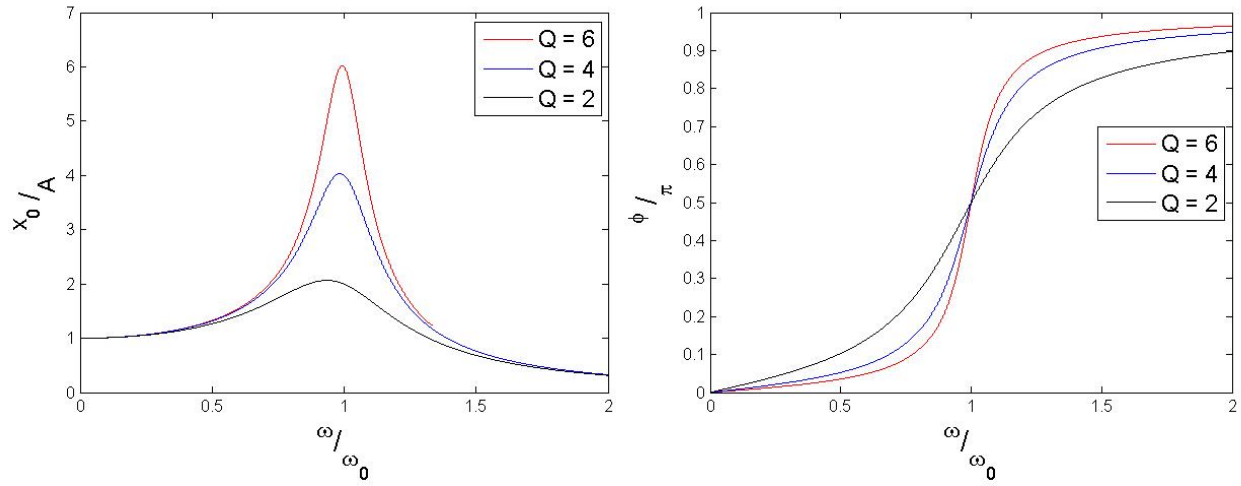

Figure 2.2: Left: The amplitude of a linear oscillator divided by the amplitude of the driving force for different frequencies of the driving force divided by the resonance frequency. Right: The phase difference between the driving force and the motion of the oscillator divided by π for different frequencies of the driving force divided by the resonance frequency.

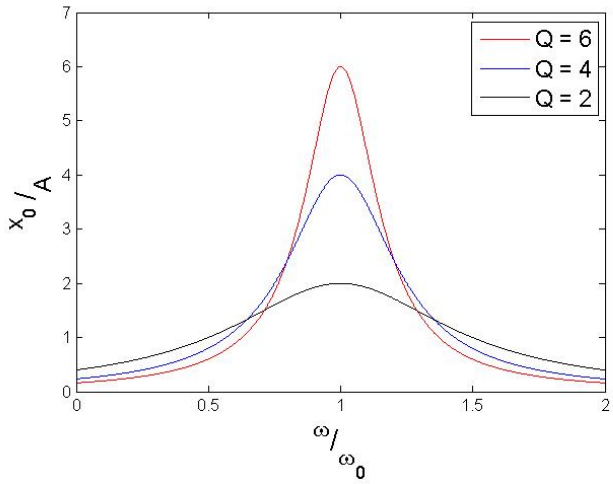

Figure 2.3: Approximation of the amplitude of a linear oscillator divided by the amplitude of the driving force for different frequencies of the driving force divided by the resonance frequency.

2.2 Nonlinear Oscillator

The derivation of the amplitude and phase equations of the nonlinear oscillator and other explanations are based on [17]. When the deformations of the a system become larger, Hooke's law (equation (2.2)) becomes too rough an approximation. A better approximation of the restoring force is given by equation (2.14).

$$F_{restoring} = -kx - \beta x^2 - \alpha x^3 \tag{2.14}$$

Also when the amplitudes of motion become larger, non-linear terms in the damping force become more important. The damping force is now approximated as:

$$F_{damping} = -l\dot{x} - \mu x\dot{x} - \eta x^2\dot{x} \tag{2.15}$$

The term β in the expression of the restoring force and the term μ in the expression of the damping force do *not* qualitatively alter the response curves of the amplitude and phase. They merely rescale the values of α and η. Therefore they will be left out in the equation of motion. The proof can be found in appendix A. Assume that the driving force has a sinusodial form. The equation of motion is now given below.

$$m\ddot{x} = \underbrace{-kx - \alpha x^3}_{\text{restoring force}} \quad \underbrace{-l\dot{x} - \eta x^2\dot{x}}_{\text{damping force}} + \underbrace{Bcos(\omega t)}_{\text{driving force}} \tag{2.16}$$

If α is positive the higher order term will assist the linear term and the oscillator will behave stiffer than described by Hooke's law. It will have a higher resonance frequency. When α is negative the oscillator will behave softer and have a lower resonance frequency compared to the resonance frequency when the higher order term is neglected. The following substitutions are made in order to make the variables dimensionless. This will result in an easier form of equation (2.16).

$$\tilde{x} = x\sqrt{\frac{\alpha}{m\omega_0^2}} \qquad and \qquad \tilde{t} = \omega_0 t \tag{2.17}$$

After the substitutions and dividing by $m\omega_0^2\sqrt{\frac{m\omega_0^2}{\alpha}}$ equation (2.18) is obtained.

$$\ddot{\tilde{x}} + \tilde{x} + \tilde{x}^3 + Q^{-1}\dot{\tilde{x}} + \tilde{\eta}\tilde{x}^2\dot{\tilde{x}} = Gcos(\tilde{\omega}\tilde{t}) \tag{2.18}$$

The relation of the dimensionless parameters with the physical ones are apart from equation (2.17) given in equation (2.19).

$$Q^{-1} = \frac{l}{m\omega_0} \qquad \tilde{\eta} = \frac{\eta\omega_0}{\alpha} \qquad G = \frac{B}{\omega_0^3}\sqrt{\frac{\alpha}{m^3}} \qquad \tilde{\omega} = \frac{\omega}{\omega_0} \tag{2.19}$$

Q is the quality factor of the oscillator.

The method of multiple scales (a perturbation method) is used to approximate the solution of equation (2.18). The method introduces a fast and a slow timescale which are treated as independent. This leads to an additional degree of freedom, which is used to remove secular[1] terms.

Now define ϵ as the reciprocal of the quality factor.

$$\epsilon = Q^{-1} \tag{2.20}$$

Note that $0 < \epsilon \ll 1$ because quality factors are often of the order 10^2 or larger. Two transformations are made concening equation (2.18).

$$G = \epsilon^{3/2}g \qquad \tilde{\omega} = 1 + \epsilon\Omega \tag{2.21}$$

Note that these transformations do not affect generality. The new form of the dimensionless equation of motion is given by equation (2.22).

$$\ddot{\tilde{x}} + \tilde{x} + \tilde{x}^3 + \epsilon\dot{\tilde{x}} + \tilde{\eta}\tilde{x}^2\dot{\tilde{x}} = \epsilon^{3/2}g\cos\left[(1+\epsilon)\tilde{t}\right] \tag{2.22}$$

The solution to equation (2.22) can be expressed as given by equation (2.23).

$$\tilde{x}(\tilde{t}) = \frac{\sqrt{\epsilon}}{2}x_0(\tilde{t}) + \epsilon^{3/2}x_1(\tilde{t}) + O(\epsilon^{5/2}) \tag{2.23}$$

[1] Secular terms are unphysical parts of a solution. They usually cause divergence when a variable approaches a certain value.

The definition of the slow and fast time are given below.

$$T_0 = \tilde{t} \qquad T_1 = \epsilon\tilde{t} \tag{2.24}$$

As dimensionless time increases the fast time increases at the same rate, while the slow time increases at a rate proportional to ϵ. The differentiating operator now becomes:

$$\frac{d}{d\tilde{t}} = \frac{\partial}{\partial T_0} + \epsilon\frac{\partial}{\partial T_1} \tag{2.25}$$

The first and second derivative of the dimensionless position are given by equations (2.26a) and (2.26b). Terms of order $\epsilon^{5/2}$ and higher are neglected.

$$\frac{d\tilde{x}}{d\tilde{t}} = \frac{\sqrt{\epsilon}}{2}\frac{\partial x_0}{\partial T_0} + \epsilon^{3/2}\left[\frac{\partial x_1}{\partial T_0} + \frac{1}{2}\frac{\partial x_0}{\partial T_1}\right] + O(\epsilon^{5/2}) \tag{2.26a}$$

$$\frac{d^2\tilde{x}}{d\tilde{t}^2} = \frac{\sqrt{\epsilon}}{2}\frac{\partial^2 x_0}{\partial T_0^2} + \epsilon^{3/2}\left[\frac{\partial^2 x_1}{\partial T_0^2} + \frac{\partial^2 x_0}{\partial T_0 \partial T_1}\right] + O(\epsilon^{5/2}) \tag{2.26b}$$

The expressions above are now inserted into equation (2.22).

$$\begin{aligned}\frac{\sqrt{\epsilon}}{2}\frac{\partial^2 x_0}{\partial T_0^2} + \epsilon^{3/2}\frac{\partial^2 x_1}{\partial T_0^2} + \epsilon^{3/2}\frac{\partial^2 x_0}{\partial T_0 T_1} + \frac{\sqrt{\epsilon}}{2}x_0 + \epsilon^{3/2}x_1 + \left(\frac{\sqrt{\epsilon}}{2}x_0 + \epsilon^{3/2}x_1\right)^3 + \epsilon\left(\frac{\sqrt{\epsilon}}{2}\frac{\partial x_0}{\partial T_0} + \epsilon^{3/2}\frac{\partial x_1}{\partial T_0}\right.\\ \left. + \frac{\epsilon^{3/2}}{2}\frac{\partial x_0}{\partial T_1}\right) + \tilde{\eta}\left(\frac{\sqrt{\epsilon}}{2}x_0 + \epsilon^{3/2}x_1\right)^2\left(\frac{\sqrt{\epsilon}}{2}\frac{\partial x_0}{\partial T_0} + \epsilon^{3/2}\frac{\partial x_1}{\partial T_0} + \frac{\epsilon^{3/2}}{2}\frac{\partial x_0}{\partial T_1}\right) = \epsilon^{3/2}gcos(T_0 + T_1\Omega)\end{aligned} \tag{2.27}$$

Comparing the coefficients for $\sqrt{\epsilon}$ and $\epsilon^{3/2}$ gives:

$$\frac{\partial^2 x_0}{\partial T_0^2} + x_0 = 0 \tag{2.28a}$$

$$\frac{\partial^2 x_1}{\partial T_0^2} + x_1 = -\frac{\partial^2 x_0}{\partial T_0 \partial T_1} - \frac{1}{8}x_0^3 - \frac{1}{2}\frac{\partial x_0}{\partial T_0} - \frac{\tilde{\eta}x_0^2}{8}\frac{\partial x_0}{\partial T_0} + g\cos(T_0 + T_1\Omega) \tag{2.28b}$$

Equation (2.28a) has the general solution:

$$x_0 = A(T_1)e^{jT_0} + c.c. \tag{2.29}$$

Equation (2.28b) is rewritten with the help of equation (2.29).

$$\frac{\partial^2 x_1}{\partial T_0^2} + x_1 = \underbrace{-\left[j\left(\frac{dA}{dT_1} + \frac{1}{2}A + \frac{\tilde{\eta}}{8}A^2A^*\right) + \frac{3}{8}A^2A^* - \frac{g}{2}e^{jT_1\Omega}\right]e^{jT_0}}_{\text{Secular term}} - \frac{1}{8}A^3e^{3jT_0} - \frac{\tilde{\eta}}{8}A^3je^{3jT_0} + c.c. \tag{2.30}$$

The left side of equation (2.30) can be seen as an undamped linear oscillator and the right side as the driving force. The first part of the right side term, indicated with the accolade, is driving at the resonance frequency. Since there is no damping term this will cause the amplitude of the oscillation to become infinite. The secular term is forced to be zero.

$$-\left[j\left(\frac{dA}{dT_1} + \frac{1}{2}A + \frac{\tilde{\eta}}{8}A^2A^*\right) + \frac{3}{8}A^2A^* - \frac{g}{2}e^{jT_1\Omega}\right]e^{jT_0} = 0 \tag{2.31}$$

Rewrite equation (2.31).

$$\frac{dA}{dT_1} = -\frac{1}{2}A - \frac{\tilde{\eta}}{8}A^2A^* + \frac{3}{8}jA^2A^* - \frac{g}{2}je^{jT_1\Omega} \tag{2.32}$$

A steady state solution of the form below is tried.

$$A(T_1) = ae^{j\Omega T_1 + \phi}, \quad a \,\epsilon\, \mathbb{R} \tag{2.33}$$

With the help of equation (2.23) and (2.29) it now follows that is $\tilde{x}(\tilde{t})$ of the form:

$$\tilde{x}(\tilde{t}) = a\sqrt{\epsilon}\cos(\tilde{\omega}\tilde{t} + \phi) + O(\epsilon^{3/2}) \tag{2.34}$$

Substituting this in equation (2.32) gives the implicit relations for the amplitude and phase of the first order term of $\tilde{x}(\tilde{t})$.

$$|a|^2 = \frac{g^2}{\left(2\Omega - \frac{3}{4}|a|^2\right)^2 + \left(1 + \frac{1}{4}\tilde{\eta}|a|^2\right)^2} \tag{2.35a}$$

$$\phi = \arctan\left(\frac{1 + \frac{1}{4}\tilde{\eta}|a|^2}{2\Omega - \frac{3}{4}|a|^2}\right) \tag{2.35b}$$

Equations (2.35a) and (2.35b) are rewritten so that it consists of the original physical quantities.

$$x_0^2 = \frac{\left(\frac{B}{2m\omega_0^2}\right)^2}{\left(\frac{\omega-\omega_0}{\omega_0} - \frac{3}{8}\frac{\alpha}{m\omega_0^2}x_0^2\right)^2 + \left(\frac{1}{2}Q^{-1} + \frac{1}{8}\frac{\eta}{m\omega_0}x_0^2\right)^2} \tag{2.36a}$$

$$\phi = \arctan\left(\frac{\frac{l}{2} + \frac{\eta}{8}x_0^2}{m\omega - m\omega_0 - \frac{3\alpha}{8\omega_0}x_0^2}\right) \tag{2.36b}$$

The image on the left shows the scaled dimensionless amplitude (equation (2.35a)) as a function of the frequency Ω. Equation (2.35a) has three solutions for a given frequency, three real solutions or one real solution and two complex solutions. The dimensionless nonlinear damping term $\tilde{\eta}$ is varied. The right image shows the phase difference between the driving force and the motion of the oscillator (equation (2.35b)). When α is taken negative (equation (2.14)) the peaks of the amplitude will bend to the left and the phase will change by 180 degrees. In order to find an expression for the resonance frequency the amplitude function (equation (2.35a)) is differentiated with respect to Ω.

$$\left[\frac{3}{64}(9 + \tilde{\eta}^2)|a|^4 + \frac{1}{4}(\tilde{\eta} - 6\Omega)|a|^2 + \frac{1}{4} + \Omega^2\right] d|a|^2 = \left[\frac{3}{4}|a|^4 - 2\Omega|a|^2\right] d\Omega \tag{2.37}$$

Setting $d|a|^2/d\Omega$ to zero gives:

$$\Omega_{max} = \frac{3}{8}|a|^2_{max} \tag{2.38}$$

Equation (2.38) is rewritten in the original physical quantities.

$$\omega_{max} = \omega_0 + \frac{3}{8}\frac{\alpha}{m\omega_0}X^2_{max} \tag{2.39}$$

Where X_{max} is the amplitude of the first order term of equation (2.23). Rewrite equation (2.39) to get an explicit expression for α.

$$\boxed{\alpha = \frac{8}{3}\frac{m\omega_0}{X^2_{max}}(\omega_{max} - \omega_0)} \tag{2.40}$$

The result agrees with the expectation. When α is zero the frequency where the amplitude is at the maximum occurs at ω_0. The resonance frequency is in this case equal to the resonance frequency of the linear oscillator. When α is positive the oscillator behaves stiffer and the resonance frequency is indeed higher according to equation (2.40). A negative α produces a lower resonance frequency.

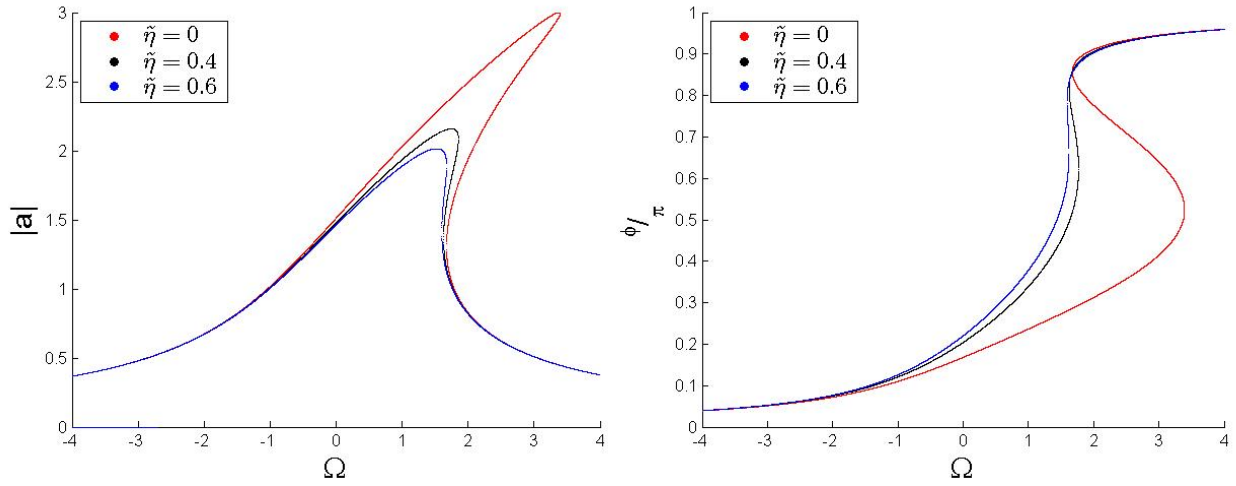

Figure 2.4: Left: The dimensionless amplitude of a nonlinear oscillator for different frequencies. Right: The phase difference between the driving force and the motion of the oscillator divided by π for different frequencies Ω.

At the bifurcation points, where the number of solutions changes from one to three or from three to one, $d\Omega/d|a|^2 = 0$.

$$\frac{3}{64}(9+\tilde{\eta}^2)|a|^4 + \frac{1}{4}(\tilde{\eta} - 6\Omega)|a|^2 + \frac{1}{4} + \Omega^2 = 0 \tag{2.41}$$

Solving for Ω gives:

$$\Omega^{\pm}_{bifurcation} = \frac{3}{4}|a|^2 \pm \frac{1}{2}\sqrt{\frac{3}{16}(3-\tilde{\eta}^2)|a|^4 - \tilde{\eta}|a|^2 - 1} \tag{2.42}$$

2.3 Optical Cavity

The discussion and derivations of the optical cavity are based on [10] and [9]. A general schematic description of an optical cavity is discussed below. An optical cavity is created by placing two highly reflective mirrors in front of eachother. To the left of the left mirror a laser is positioned. Assume that the light of the laser is

Figure 2.5: A schematic setup of an optical cavity.

monochromatic. The light emitted by the laser may be transmitted into the cavity or may be reflected by the mirror. The frequencies of the laserlight which leads to a large transmittance are the resonance frequencies of the cavity.

$$\omega_m = m\frac{\pi c}{L}, \quad m = 1, 2, 3, ... \tag{2.43}$$

m is called the mode number and L is the length of the cavity. The separation between the resonance frequencies is called the free spectral range.

$$\Delta\omega_{FSR} = \pi\frac{c}{L} \tag{2.44}$$

Due to the high reflectivity of the mirrors the photons inside the cavity "bounce" between the mirrors. Imperfections of the cavity cause internal absorption of photons and photons are scattered out of the cavity. These leads to a decay rate of the photons in the cavity. The decay rate is denoted as κ. Another useful quantity is the optical finesse: $\mathcal{F}$.

$$\mathcal{F} = \frac{\Delta\omega_{FSR}}{\kappa} \tag{2.45}$$

The optical finesse is equal to the average number of roundtrips of the photons in the cavity times 2π. It is a dimensionless parameter that gives information about the quality of the cavity. An alternative for the optical finesse is the quality factor of the cavity.

$$Q_{opt} = \omega_{cav}\tau \tag{2.46}$$

τ is the average lifetime of the photon in the cavity ($\tau = \kappa^{-1}$). The decay rate is ussually divided in an external and an internal part. The external decay rate, κ_{ex}, represents losses that are caused outside the cavity. For example: if the transmission condition is met, some light still gets reflected of the left cavity mirror. The internal part, κ_0, represents losses that are caused inside the cavity. For example: absortion of photons inside the cavity, scattering of photons from the inside to the outside of the cavity and transmission of photons through the right cavity mirror.

$$\kappa = \kappa_{ex} + \kappa_0 \tag{2.47}$$

The input-output relation is now discussed. $\hat{a}_{in}$ denotes the field amplitude to the left of the left mirror, $\hat{a}$ the field amplitude inside the cavity and $\hat{a}_{out}$ the field amplitude to the right of the right mirror. The input and output field amplitudes must satisfy equation (2.48).

$$\hat{a}_{out} = \hat{a}_{in} - \sqrt{\kappa_{ex}}\hat{a} \tag{2.48}$$

The Heisenberg equation of motion for the field amplitude is given by:

$$\dot{\hat{a}} = -\frac{\kappa}{2}\hat{a} + i\Delta\hat{a} + \sqrt{\kappa_{ex}}\hat{a}_{in} \tag{2.49}$$

In equation (2.49): $\Delta = \omega_L - \omega_c$, the amount of detuning of the laser from the cavity resonance frequency. The field amplitude $\hat{a}_{in}$ is normalized such that the input power is given by $\hbar\omega\,|\langle\hat{a}_{in}\rangle|^2$. (The angle brackets represent an average). When the optical cavity is at steady state: $\dot{\hat{a}} = 0$. Equation (2.48) and equation (2.49) can be combined to get a relation between the average field amplitude in the optical cavity and the average field amplitude to the left of the left mirror.

$$\langle\hat{a}\rangle = \frac{\sqrt{\kappa_{ex}}\,\langle\hat{a}_{in}\rangle}{\frac{\kappa}{2} - i\Delta} \tag{2.50}$$

The average number of photons "bouncing" in optical cavity is given by:

$$\langle n_{cav}\rangle = |\langle a\rangle|^2 = \frac{\kappa_{ex}}{\Delta^2 + (\kappa/2)^2}|\,\langle\hat{a}_{in}^2\rangle\,| = \frac{\kappa_{ex}}{\Delta^2 + (\kappa/2)^2}\frac{P}{\hbar\omega_L} \tag{2.51}$$

With the help of equation (2.47),(2.48) and (2.50) a formula for $\langle\hat{a}_{out}\rangle\,/\,\langle\hat{a}_{in}\rangle$ and it's phase is found.

$$R = \frac{\langle\hat{a}_{out}\rangle}{\langle\hat{a}_{in}\rangle} = \frac{(\kappa_0 - \kappa_{ex})/2 - i\Delta}{(\kappa_0 + \kappa_{ex})/2 - i\Delta} \tag{2.52a}$$

$$\phi = \arctan\left(\frac{4\Delta\kappa_{ex}}{\kappa_0^2 - \kappa_{ex}^2 + 4\Delta^2}\right) \tag{2.52b}$$

The reflection coefficient is now:

$$\Gamma = \frac{|\langle\hat{a}_{out}\rangle|^2}{|\langle\hat{a}_{in}\rangle|^2} = \frac{\kappa_0^2 + \kappa_{ex}^2 - 2\kappa_0\kappa_{ex} + 4\Delta^2}{\kappa_0^2 + \kappa_{ex}^2 + 2\kappa_0\kappa_{ex} + 4\Delta^2} \tag{2.53}$$

Three regimes based on the internal and external dacay rate are distinguished. If $\kappa_{ex} \gg \kappa_0$ the reflection is almost equal to 1. The cavity is said to be overcoupled. Almost all the photons from the laser come back out of the cavity without being absorbed, scattered or transmitted. The case where $\kappa_{ex} = \kappa_0$ refers to critical coupling. The reflection coefficient is 0 at the resonance frequencies ($\Delta = 0$). The input power must be dissipated inside the cavity or fully transmitted through the right mirror. The last possibility is $\kappa_{ex} \ll \kappa_0$. The cavity is said to be undercoupled. Photons are mostly lost inside the cavity. To more easily refer to the kind of coupling, the coupling efficiency is introduced.

$$\eta = \frac{\kappa_{ex}}{\kappa} \tag{2.54}$$

Values of $1/2 < \eta \leq 1$ indicate overcoupling, $\eta = 1/2$ critical coupling and $0 \leq \eta < 1/2$ undercoupling. The left image in figure 2.6 shows a plot of the reflection coefficient for different values of η. The undercoupling regime shows a sharp dip at the resonance frequency, indicating that the reflection quickly goes to one when the laser is more detuned. The overcoupling regime shows a much broader dip. In the right figure the minimum of the reflection is plotted as a function of the coupling efficiency. At critical coupling the minimum of the reflection goes to zero and for over- and undercoupling the minimum goes at the same pace to higher values.

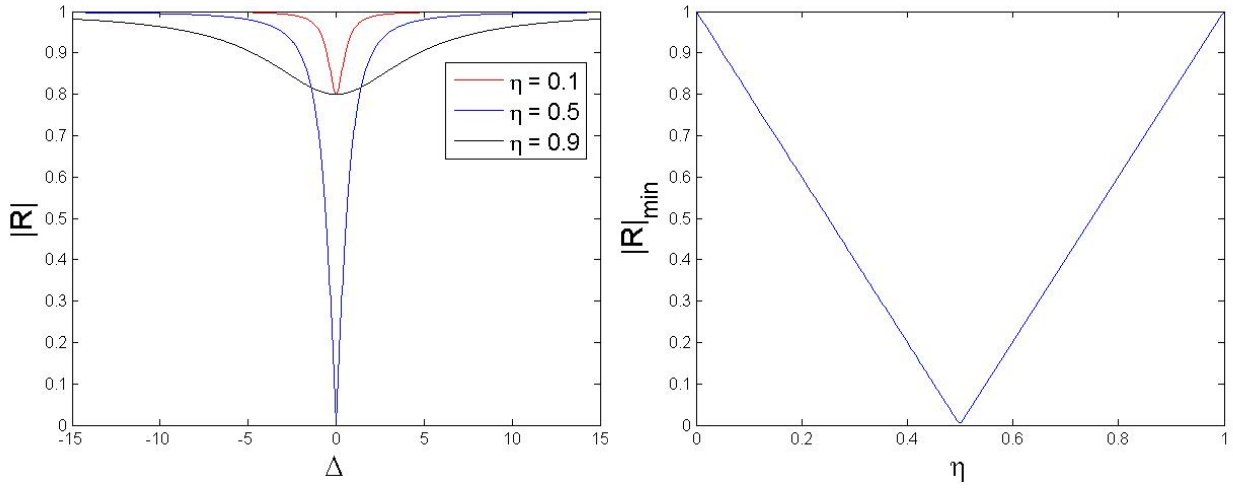

Figure 2.6: Left: The reflection versus the detuning of the laser for different couling regimes. Right: The minimum of the reflection versus the coupling efficiency.

2.4 Microwave resonators

The wavelength of microwaves with frequency of order GHz is a few mm. The microwave cavity can be made in this frequency range by terminating a transmissionline of a quarter or half wavelength. A discussion and derivations regarding transmissionlines is included in appendix B. In this research the superconducting cavity is a quarter wavelength coplanar waveguide resonator. As shown in the appendix the inductance and capacitance per unit length can be tuned such that the resonance frequency is in the few GHz range.

2.5 Optomechanics

The discussion and derivations in this section are based on [9] and [18]. Now suppose the right mirror of the optical cavity is connected to a mechanical oscillator. The left mirror remains fixed, see figure 2.8. The movement of the mechanical oscillator will change the length of the cavity and thus the transmittance

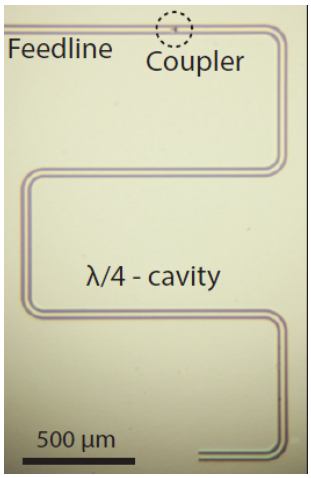

Figure 2.7: A schematic setup of an optical cavity.

condition. The signal of the detector contains information about the motion of the oscillator. Assume that the oscillator has a frequency of ω_m. When a photon is reflected momentum of $|\Delta p| = 2h/\lambda$ is transfered.

Figure 2.8: A schematic setup of an optomechanical system.

The force caused by the radiation pressure is given by:

$$\langle F \rangle = \frac{2h}{\lambda} \cdot \frac{1}{\tau_c} \cdot \langle n_{cav} \rangle = \frac{\hbar\omega}{L} |\langle \hat{a} \rangle|^2 = \hbar G |\langle \hat{a} \rangle|^2 \tag{2.55}$$

Where $\tau_c = 2L/c$, the time it takes the photon to make a roundtrip in the cavity and G is the frequency pull parameter, the change of resonance frequency due to change in position. From equation (2.55) it is clear that the radiation pressure force decreases when the lenght of the cavity increases. The oscillator experiences the momentum transfer as a radiation pressure from the light inside the cavity. The movement of the oscillator results in more or less light in the cavity and thus in more or less radiation pressure. The motion of the right mirror influences itself by changing the radiation pressure it experiences. This is called dynamical backaction.

Due to the particle nature of light the laser exhibits shot noise. The number of photons emitted by the laser fluctuates. The leads to variations in the radiation pressure. If the intensity of the laser increases the signal to noise ratio improves. Higher laser intensities leads to more photons in the cavity and gives a higher radiation pressure. Optimum sensitivity is achieved at the standard quantum limit (SQL). At the SQL the contribution of the shot noise and quantumback action are both equal to half of the zero-point motion the right mirror ($x_{zpf} = \sqrt{\frac{\hbar}{2m\omega_m}}$).

Because the right mirror is now connected to a mechanical oscillator, the equation for the field amplitude (equation (2.49)) has to be modified.

$$\dot{\hat{a}} = -\frac{\kappa}{2}\hat{a} + i(\Delta - G\hat{x})\hat{a} + \sqrt{\kappa_{ex}}\hat{a}_{in} \tag{2.56}$$

We also write down the equation of motion of the oscillator in the linear regime.

$$m_{eff}\ddot{\hat{x}} = -m_{eff}\omega_m^2\hat{x} - m_{eff}\Gamma_m\dot{\hat{x}} - \hbar G|\langle\hat{a}\rangle|^2 \tag{2.57}$$

Equation (2.56) and equation (2.57) are linearized around a steady state solution: $\hat{a} = \bar{a}+\delta\hat{a}$ and $\hat{x} = \bar{x}+\delta\hat{x}$.In order to find $\bar{a}$ and $\bar{x}$, the derivatives $\dot{\hat{a}}$, $\ddot{\hat{x}}$ and $\dot{\hat{x}}$ are set to zero in equation (2.56) and equation (2.57).

$$\bar{a} = \frac{\sqrt{\kappa_{ex}}\hat{a}_{in}}{\frac{\kappa}{2} - i(\Delta - G\bar{x})} \tag{2.58a}$$

$$\bar{x} = \frac{\hbar G|\langle\hat{a}\rangle|^2}{m_{eff}\omega_m^2} \tag{2.58b}$$

Substituting $\hat{a} = \bar{a} + \delta\hat{a}$ and $\hat{x} = \bar{x} + \delta\hat{x}$ in equation (2.56) and equation (2.57) gives:

$$\frac{d}{dt}\delta\hat{a} = (i\bar{\Delta} - \frac{\kappa}{2})\delta\hat{a} - iG\bar{a}\delta\hat{x} + \sqrt{\kappa_{ex}}\delta\hat{a}_{in} \tag{2.59a}$$

$$\frac{d^2}{dt^2}\delta\hat{x} + \Gamma_m\frac{d}{dt}\delta\hat{x} + \omega_m^2\delta\hat{x} = -\frac{\hbar G}{m_{eff}}(\delta\hat{a} + \delta\hat{a}^\dagger) \tag{2.59b}$$

Where $\bar{\Delta} = \Delta - G\bar{x}$ and only first order terms in the quantities $\delta\hat{a}$ and $\delta\hat{x}$ are retained. We assume that $\delta\hat{a}_{in}$ can be written as: $\delta\hat{a}_{in} = s_p e^{-i(\omega_p-\omega_d)t} = s_p e^{-i\Omega t}$. Here ω_p is the probe frequency, ω_d the drive frequency (see the experimental set-up section) and s_p the number of photons as a function of the probe power. Another Ansatz is introduced:

$$\delta\hat{a}(t) = A^- e^{-i\Omega t} + A^+ e^{+i\Omega t} \tag{2.60a}$$

$$\delta\hat{a}^\dagger(t) = (A^+)^* e^{-i\Omega t} + (A^-)^* e^{i\Omega t} \tag{2.60b}$$

$$\delta\hat{x}(t) = X e^{-i\Omega t} + X^* e^{i\Omega t} \tag{2.60c}$$

Equation (2.60a) and equation (2.60c) are substituted into equation (2.59a). Comparing coefficients for $e^{-i\Omega t}$ and $e^{i\Omega t}$ gives:

$$-i\Omega A^- = \left(i\bar{\Delta} - \frac{\kappa}{2}\right)A^- - iG\bar{a}X + \sqrt{\kappa_{ex}}s_p \tag{2.61a}$$

$$i\Omega A^+ = (i\bar{\Delta} - \frac{\kappa}{2})A^+ - iG\bar{a}X^* \tag{2.61b}$$

Equations (2.60a), (2.60b) and (2.60c) are substituted into equation (2.59b). Comparing coefficients for $e^{-i\Omega t}$ and $e^{i\Omega t}$ gives:

$$X(-\Omega^2 - i\Omega\Gamma_m + \omega_m^2) = -\frac{\hbar G}{m_{eff}}(A^- + (A^+)^*) \tag{2.62a}$$

$$X^*(-\Omega^2 + i\Omega\Gamma_m + \omega_m^2) = -\frac{\hbar G}{m_{eff}}(A^+ + (A^-)^*) \tag{2.62b}$$

From equations (2.61a) and (2.61b):

$$A^- = \frac{iG\bar{a}X - \sqrt{\kappa_{ex}}s_p}{i(\Omega + \bar{\Delta}) - \frac{\kappa}{2}} \tag{2.63a}$$

$$A^+ = \frac{-iG\bar{a}X^*}{i(\Omega - \bar{\Delta}) + \frac{\kappa}{2}} \tag{2.63b}$$

Equations (2.63a) and (2.63b) are substituted in equation (2.62a). Equation (2.62b) is needed to rewrite the result.

$$X = \frac{\hbar G\bar{a}\chi(\Omega)\sqrt{\kappa_{ex}}s_p}{i(\bar{\Delta} + \Omega) - \frac{\kappa}{2} - 2\bar{\Delta}f(\Omega)} \tag{2.64}$$

Where:

$$f(\Omega) = \hbar G^2 \bar{a}^2 \frac{\chi(\Omega)}{i(\bar{\Delta} - \Omega) + \frac{\kappa}{2}} \tag{2.65a}$$

$$\chi(\Omega) = \frac{1}{m_{eff}} \cdot \frac{1}{\Omega_m^2 - \Omega^2 - i\Omega\Gamma_m} \tag{2.65b}$$

Also the following two equations hold.

$$s_p = \frac{\sqrt{\kappa_{ex}}}{\kappa/2} \cdot \sqrt{\frac{P_{probe}}{\hbar\omega_c}} \tag{2.66}$$

$$A^- = s_p(1 - |S_{11}|) \tag{2.67}$$

Here S_{11} is the measured reflection.

Now the equation for the amplitude of the mechanical resonator is:

$$\boxed{X = \chi\hbar G\bar{a}A^-} \tag{2.68}$$

Equation (2.68) will be used to calculate the amplitude of the oscillator.

For a discussion of the influence of back-action on the measured reflection see appendix C.

3 Experimental Set-up

The left image of figure 3.1 shows a falso colored picture of the device. A multilayer graphene flake, with a thickness of approximately 10 nm, forms a capacitor between the superconducting cavity and the transmissionline (feedline). This capacitor is denoted as C_m in the right image of figure 3.1. The distance between the cavity and the drum is approximately 150 nm. The mircowave photons are coupled in and out of the cavity via the transmissionline. A more detailed description of the production technique can be found in [14]. The circuit model of the superconducting cavity and the graphene resonator is shown in the right image. The ground displayed at the bottom forms one of the "mirrors" and the high impedance of the two capacitors at the top (C_1 and C_m) forms the other "mirror" (see equation (B.14) in appendix B). Low frequency RF voltages can be applied to the microwave feedline.

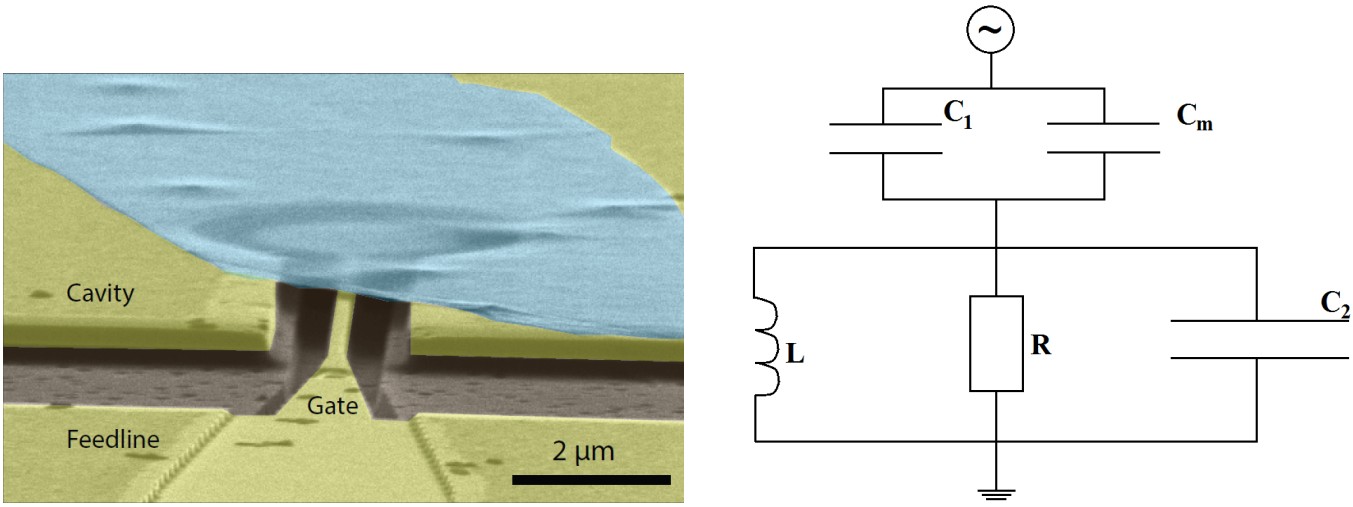

Figure 3.1: Left: False colored electron microscope image of the device. The image is taken from [14]. Right: Model of superconducting cavity with the graphene resonator. The graphene resonator is denoted as C_m.

3.1 Cavity response

Figure 4.1 shows a schematic view of the setup used to measure the cavity response. The impendance of the cavity is 50 Ω. Note that C_m is fixed and R is very large, because the cavity is cooled to a temperature of order 10 mK. To the attenuation of 39.6 dB another 40 dB is added and the cable at the input gives another 8 dB attenuation. The attenuation at the input brings the signal to a more thermalized state (smaller frequency peak). There is a frequency sweep at the input and the reflection for each frequency is measured.

Equation (2.53) applies to the ideal case. An α is introduced which gives the quality of isolation from port 1 to 3 of the circulator. There is an incoming field amplitude at port 1 of the circulator. Most of the signal goes to port 2, but some of the signal leaks directly to port 3 and skips the cavity. The signal that goes from port 1 directly to port 3 undergoes some phase shift. Figure 3.3 illustrates the process described above. Equation (2.52a) is now rewritten.

$$R = \alpha e^{i\phi} + (1-\alpha)\left(1 - \frac{\kappa_{ex}}{\kappa/2 - i\Delta}\right) \tag{3.1}$$

Squaring equation (3.1) gives:

$$R^2 = \alpha^2 + 2\alpha(1-\alpha)\cos(\phi) + (1-\alpha)^2 + \frac{4(\alpha-1)\kappa_{ex}}{\kappa^2 + 4\Delta^2}\left[\alpha\kappa\cos(\phi) + (1-\alpha)\kappa_0 + 2\alpha\Delta\sin(\phi)\right] \tag{3.2}$$

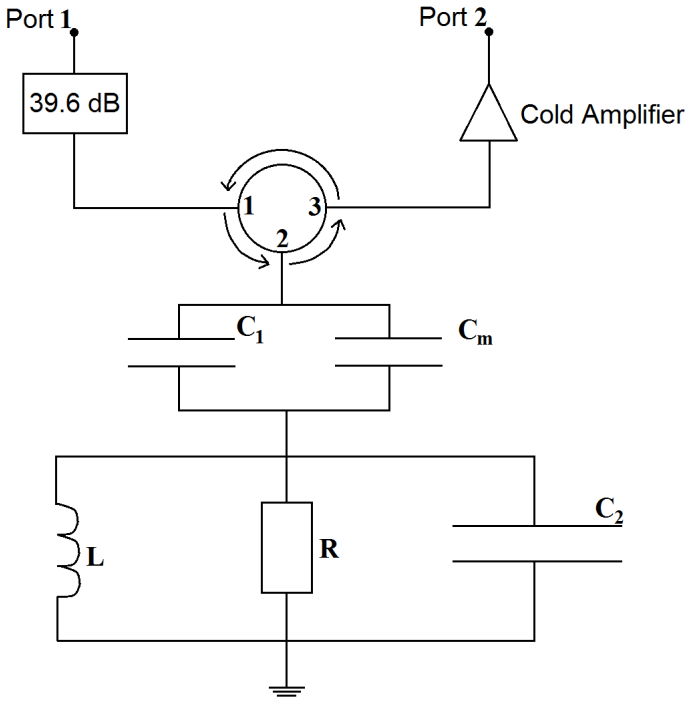

Figure 3.2: Schematic view of the setup to measure the cavity response.

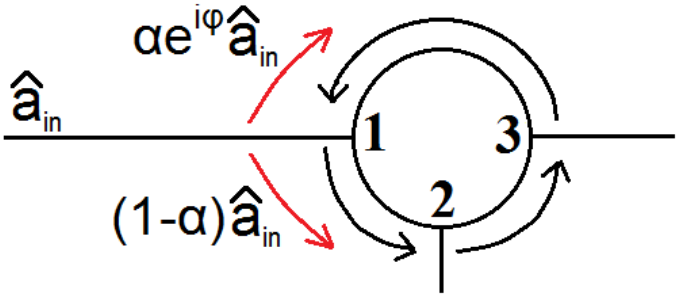

Figure 3.3: Schematic view of an imperfect circulator. An ideal circulator would have $\alpha = 0$. In practice some signal leaks across to port 3 instead of going to port 2. This is relevant for the asymmetry in figure 4.1.

The squared form (equation (3.2)) was used to make the fit and extract the parameters.

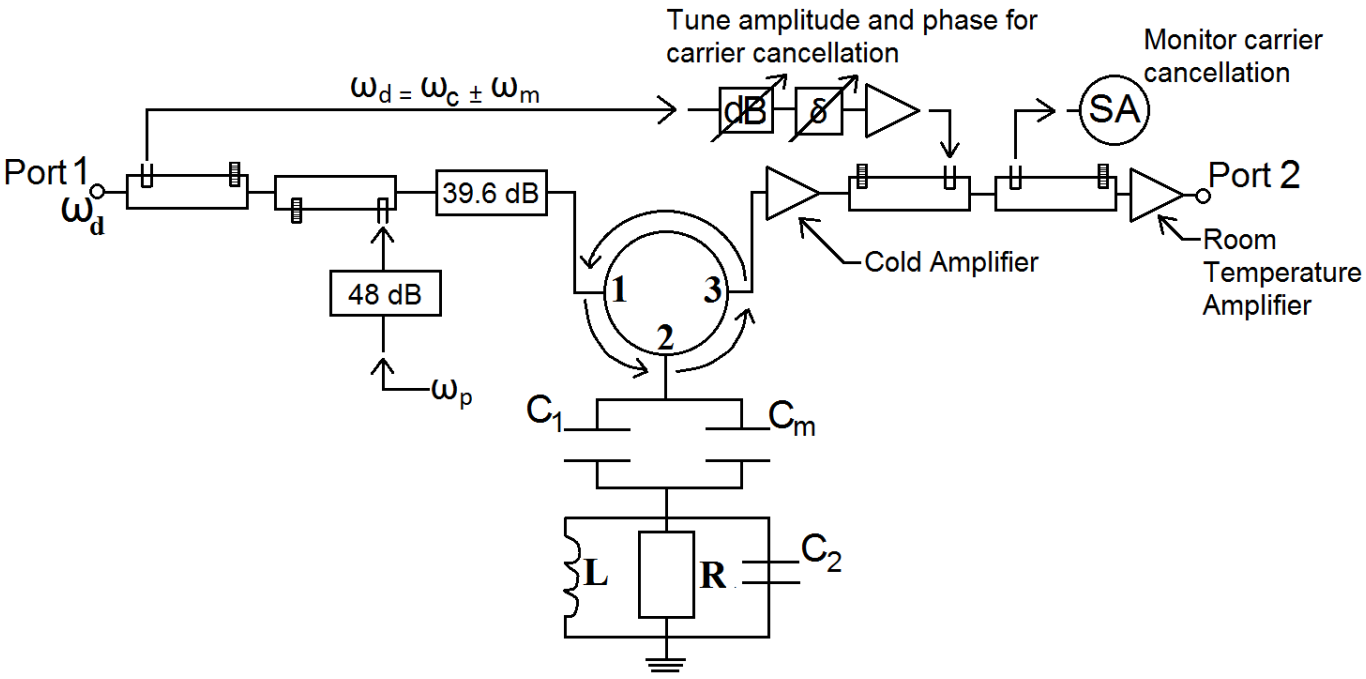

Figure 3.4: Schematic view of the setup to measure the response of the oscillating graphene layer. Signal ω_d comes in at port 1. At the first directional coupler the signal splits and a small part of the signal is used in the cancellation proces. The larger part of the signal goes on and at the second directional coupler ω_p is added. The signals combine and beat at ω_m. The carrier signal at ω_p is cancelled as much as possible by adjusting the phase and amplitude of the reference signal and monitoring the result with a spectrum analyser. The desired signal comes out at port 2.

3.2 Optomechanical induced transparancy (OMIT)

Figure 3.2 shows the schematic setup used to measure the response of the graphene oscillator. The amplifiers used in the circuit are HEMT amplifiers with a gain of 35 dB at 6 GHz. The coupling factors of the directional couplers vary. The shaded output ports of the directional couplers are closed (infinite resistance). The graphene layer is driven. This means that the C_m becomes a function of time.

The signal at the input (port 1) has a relatively large amplitude and has frequency $\omega_d = \omega_c \pm \omega_m$. If $\omega_d = \omega_c - \omega_m$ is chosen, the cavity is said to be driven at the red side band. If $\omega_d = \omega_c + \omega_m$ is chosen, the cavity is driven at the blue side band. The first directional coupler has a coupling factor of -10 dB. The small signal obtained from the side port is used as a reference signal and for cancellation. At the second directional coupler ω_p is added. The second directional coupler has a coupling factor of -20 dB. This signal is further attenuated by adding an attenuation of 48 dB. (This attenuation consists of two attenuators of 20 dB and the cable provides another 8 dB). The total signal is again attenuated by 39.6 dB in order to get a more thermalized state. The two signals ω_d and ω_p combine and beat at ω_m. Now ω_m and ω_d combine to give a signal at ω_p. In order to analyse the relevant signal the carrier signal has to be attenuated through a carrier cancellation process. The amplitude for different frequencies is monitored with a spectrum analyser. The amplitude and phase of the signal obtained from the side port of the first directional coupler are adjusted so that the signal has a low amplitude at the frequency ω_d. The signal at ω_p is now amplified.

4 Results and discussion

4.1 Cavity response measurement

Figure 4.1 shows the measurement of the reflection[2] of the microwave cavity. The asymmetry of the figure is caused by the imperfect circulator (see figure 3.3). The measurement was done at $T \approx 13\,mK$. The following parameters are estimated with the help of a least square fit:

$$\begin{aligned} \kappa_0 &= 2\pi \cdot 51.7\ kHz \\ \kappa_{ex} &= 2\pi \cdot 197.8\ kHz \\ \omega_c &= 2\pi \cdot 5.901\ GHz \\ a &= 0.064 \\ \frac{\phi}{\pi} &= -0.317 \end{aligned} \tag{4.1}$$

The cavity is in the overcoupling regime: $\eta = 0.751$.

[2] The reflection will from now on be denoted as $|S_{11}|$.

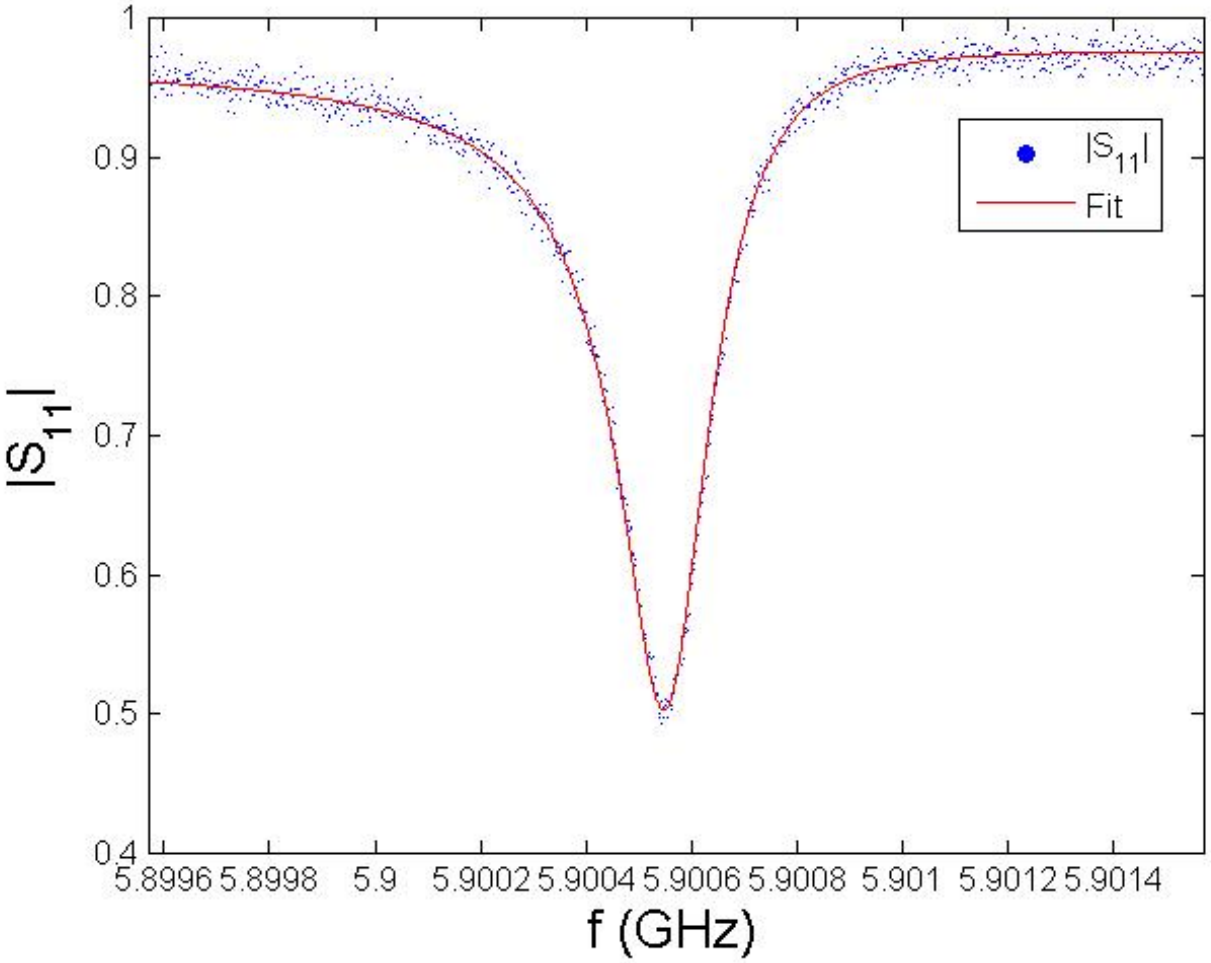

Figure 4.1: Measurement of the resonant frequency of a microwave cavity.

4.2 Linear and Non-Linear mechanics with OMIT setup.

The cavity response is used to measure mechanics. The mechanical resonator is driven by adding a small RF signal and a DC voltage to the microwave feedline. The force on the graphene layer is proportional to the pump power and probe power: $Driveforce \propto P_{pump} \cdot P_{probe}$. The cavity is driven at the red side band frequency [3]: $\omega_d = \omega_c - \omega_m = 2\pi \cdot 5.864187\ GHz$. (The blue side band would be $\omega_c + \omega_m$). A typical signal that is measured is shown in figure 4.2. The sharp dip in the middle of the large dip shows the mechanical response. We now zoom in on the sharp dip (see figure 4.3). The driving force is adjusted by changing the power of the pump and probe. It is observed that the sharp dip has a Lorenzian shape when the power of the pump and probe are set to a low value. The shape of the signal changes when the power of the pump and probe are set to a higher value. The signal gets a "shark fin" shape.

As the frequency goes up the response follows the curve as was shown in the image on the left of figure 2.4. As frequency keeps rising the curve the response was initially following bends backward in frequency and the signal drops sharply to the lower solution. This explains the "shark fin" like shape that appears.

[3]The location of the red side band frequency in the frequency domain can be found by taking a big sweep of the drive frequency.

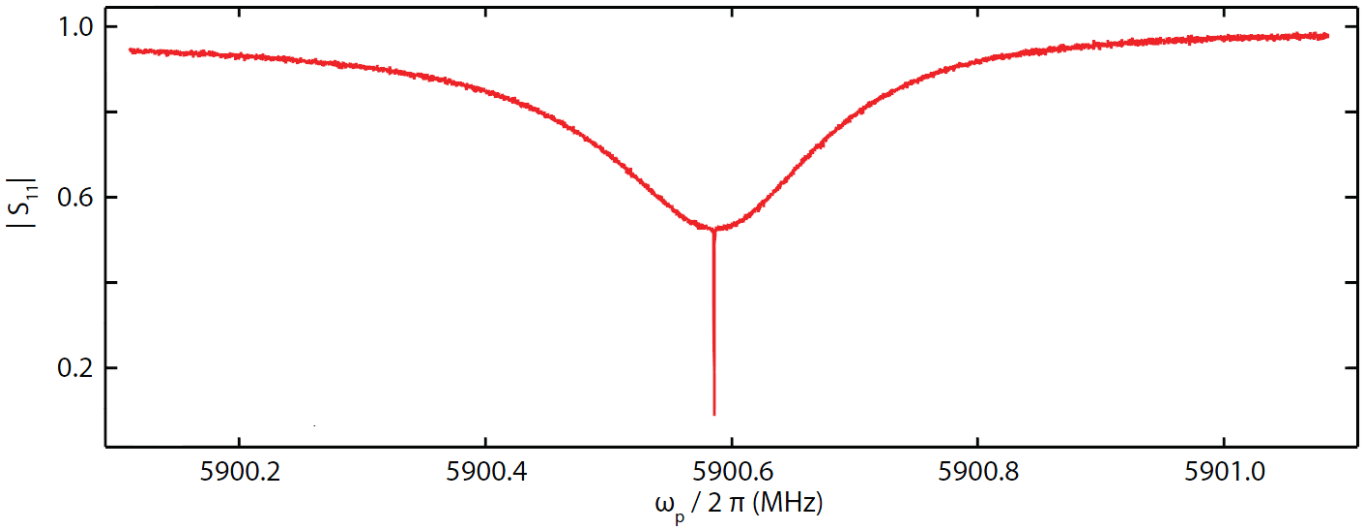

Figure 4.2: Measurement of the response when the oscillator is driven and the frequency is swept. The image is taken from [14].

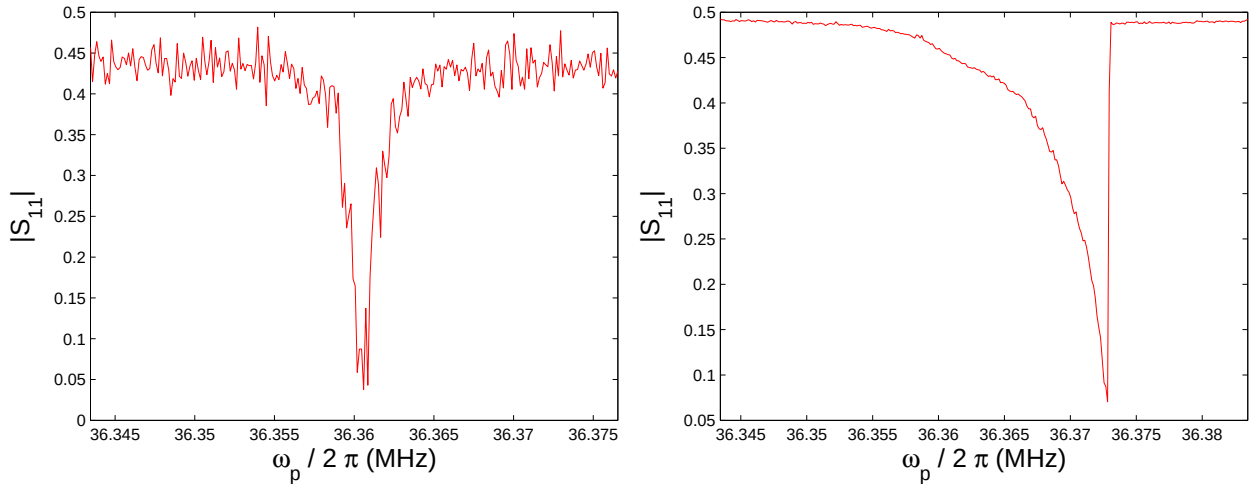

Figure 4.3: Left: Example of the signal when the driving force is low. The shape is Lorenzian. Right: Example of a signal when the driving force is high. The shape is duffing.

It is noted that the signal to noise ratio is worse a low powers. Also at low powers the signal tends to become more unstable: the peak drifts back and forth in frequency.

4.3 Vary probe power with fixed pump power at the red side band

We fix the pump power and vary the probe power. For the first probe power sweep the pump power is fixed at 14 dBm and for the second one the pump power is set to 17 dBm. The effect of backaction is small at the pump power of 14 dBm and more significant at the pump power of 17 dBm. A more extensive explanation can be found in appendix D.

4.3.1 Pump power is set to 14 dBm and the probe power is varied.

The pump power is fixed at 14 dBm and the reflection is measured at the integer probe powers between -20 dBm and 15 dBm. The frequency sweep is done in both directions: from a low to a high frequency and the other way round. At a low probe power the signal has a Lorenzian shape. The measurement with a Lorenzian shape that is the most stable is sought out and fitted with equation (2.11a) to extract the quality factor (see figure 4.8). The estimated quality factor was 148899.

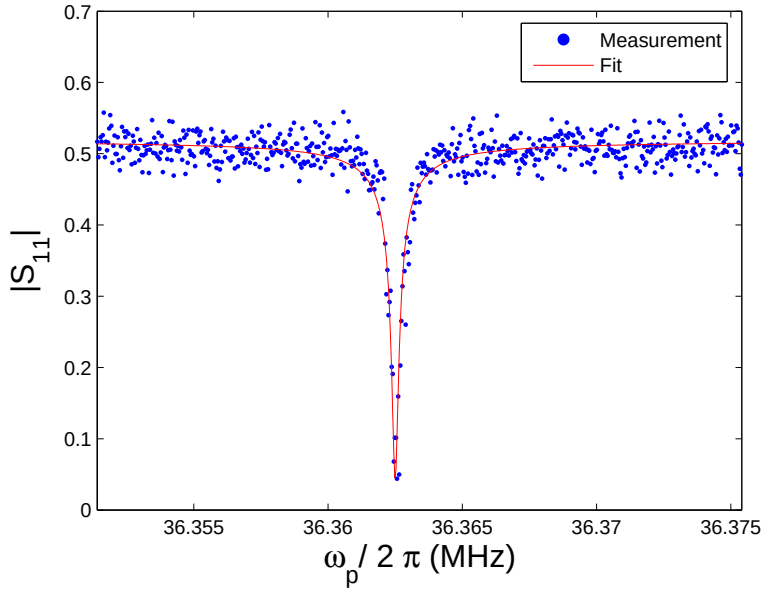

Figure 4.4: Signal and fit for a pump power of 14 dBm and a probe power of -13 dBm. The frequency was swept upwards. The quality factor was estimated to be 148899.

We now proceed to convert the measured reflections to mechanical amplitudes with equation (2.68) for the different probe powers. The values of m_{eff} and G are taken from [14].

$$\begin{aligned} m_{eff} &= 0.276\ pg \\ G &= 2\pi \cdot 26.5\ kHz/nm \end{aligned} \tag{4.2}$$

The maximal mechanical amplitude and the frequency at which this maximal amplitude occurs are determined for each of the probe powers. Figure 4.5 illustrates the situation for the linear regime and the non-linear regime.

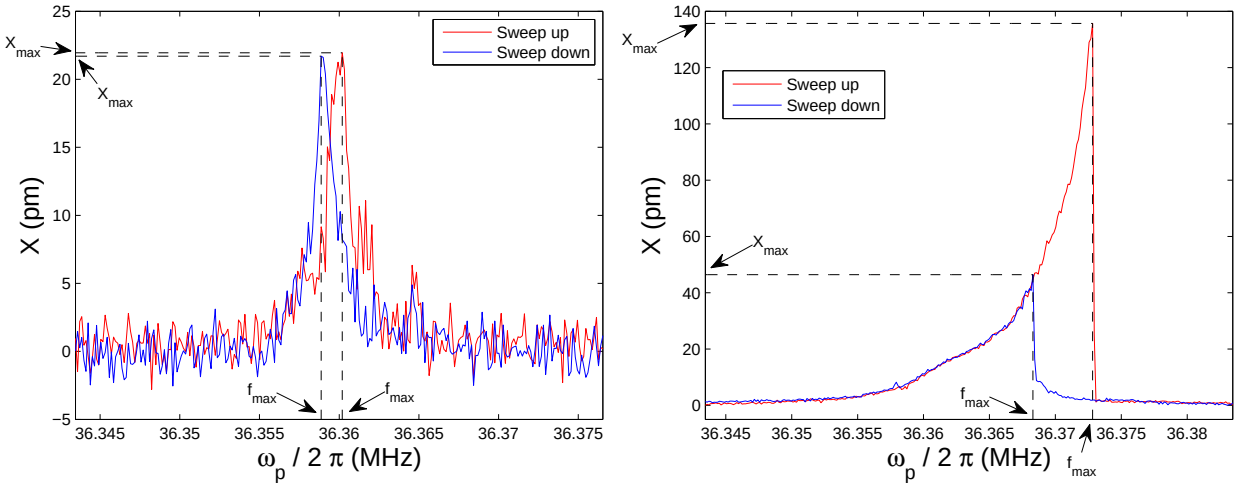

Figure 4.5: Left: Example of the mechanical response when the driving force is low. The probe power is $-16\ dBm$. The red signal corresponds with a frequency sweep in the upward direction and the blue signal with a frequency sweep in the downward direction. The maximal amplitude and the frequency at which it occurs are indicated with the help of the dotted lines. Right: Example of the mechanical response when the driving force is high. The probe power is 15 dBm.

The signal that corresponds with a low power (left image) shows a Lorentzian shape in contrast to the "shark fin" shape of the signal that corresponds with the higher power (right image). The signal observed at low probe powers tended to become more unstable. The dip drifts back and forth in frequency. This can be seen in the images, the dips should have occured at the same frequency if the signal was stable. Also is the signal to noise ratio worse at low powers.

It is noticed in the right image of figure 4.5 that the height of the dips differs a lot. This can be explained with figure 2.4 in mind. When frequency is swept in the direction of the bending of the amplitude the signal will follow the upper branch and when the amplitude tends to bend back in frequency, the signal bifurcates to the lower solution. This will result in the large amplitude. When frequency is swept from the other direction, the lower branch is followed until the amplitude tends to bent back in frequency, then the signal bifurcates to the upper solution. This will result in a lower amplitude. When the frequency is swept from a low to a high frequency the bifurcation frequency is larger than the bifurcation frequency that correponds with a sweep from a high to a low frequency as can be seen in figure 2.4. This is reflected in the right image of figure 4.5 where the sharp jump from the maximal amplitude tot the background signal occurs at a larger frequency for the forward frequency sweep and earlier in frequency for the backward frequency sweep. To illustrate the difference between the sweep up and the sweep down measurements figure 4.6 is included. It shows the frequency where the amplitude is maximal as a function of probe power.

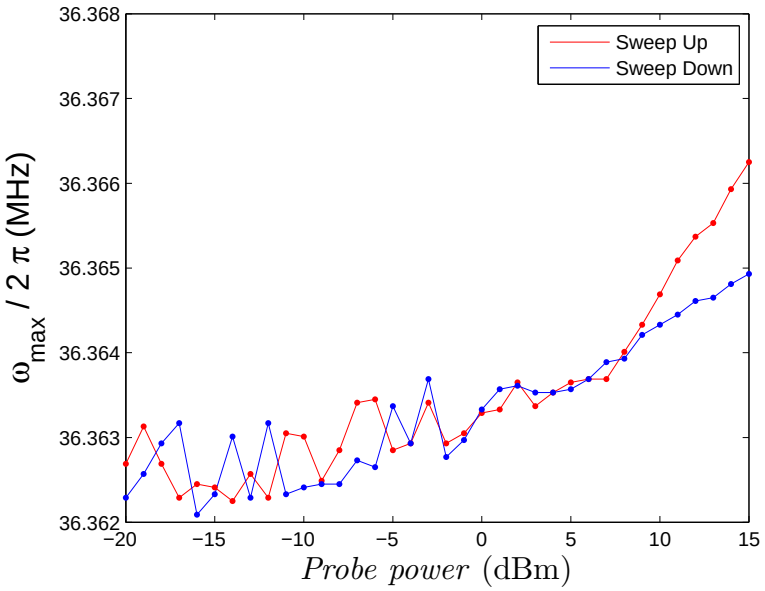

Figure 4.6: Frequency at which the maximal amplitude occurs for the different probe powers and a fixed pump power of 14 dBm. At large probe powers the amplitude response bends sharper (becomes more duffing) which results in a bigger difference between the bifurcation frequencies of the sweep up and sweep down measurement.

The frequency at which the maximum amplitude occurs, is plotted as a function of the mechanical amplitude squared for each of the probe powers for the upward sweep measurements. The result should be a straight line according to equation (2.39) with slope equal to $\frac{3}{8}\frac{\alpha}{m\omega_0}$. Equation (2.39) is only valid for the sweep up measurements[4]. The value of α is estimed by making a linear fit through the measurement points and setting the slope of the fit equal to $\frac{3}{8}\frac{\alpha}{m\omega_0}$. The estimated value of α is $3.3 \cdot 10^{16}\ kg/m^2s^2$.

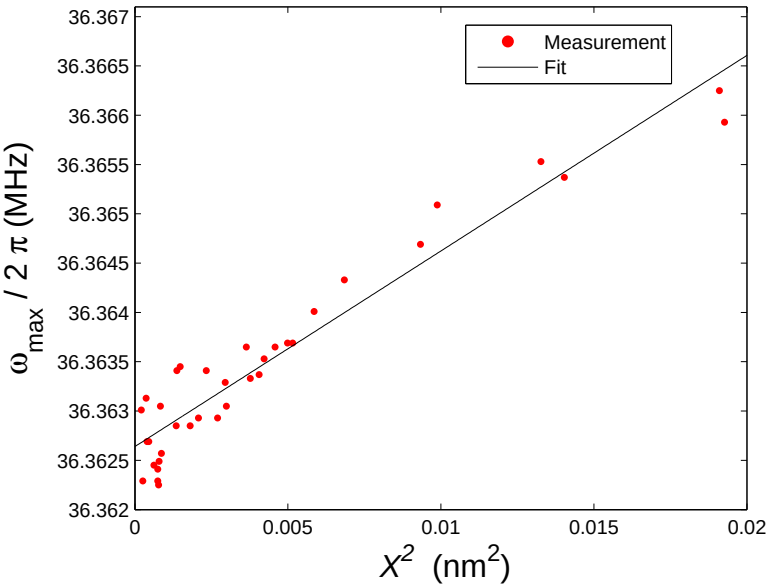

Figure 4.7: The frequency at which the amplitude is maximal as a function of the maximal amplitude squared. The pump power is 14 dBm and the probe powers vary between -20 and 15 dBm. The measurement points are fitted with a straight line in accordance with equation 2.39. By setting the slope equal to $\frac{3}{8}\frac{\alpha}{m\omega_0}$ the value of α is estimated to be $3.3 \cdot 10^{16}\ kg/m^2s^2$.

4.3.2 Pump power is set to 17 dBm and the probe power is varied.

The pump power is now fixed at 17 dBm and the probe is varied again. The reflection is measured at the integer probe powers between -20 dBm and 15 dBm. The frequency sweeps are again done in both directions. The measurement with a Lorentzian shape that is most stable is sought out and fitted with equation 2.11a. This yields a quality factor of 62769.

[4]This is because equation (2.39) was derived by setting $d|a|^2/d\Omega$ to zero.

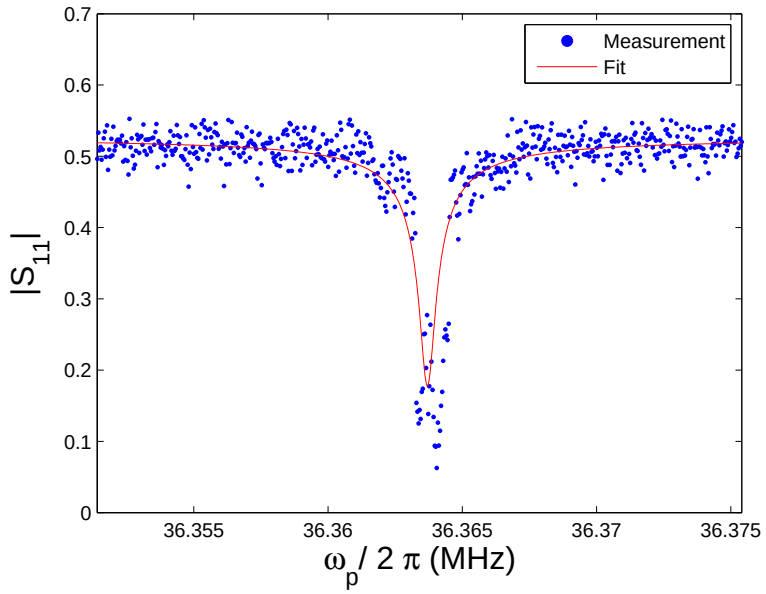

Figure 4.8: Signal and fit for a pump power of 17 dBm and a probe power of -18 dBm. The frequency was swept upwards. The quality factor was estimated to be 62769.

Next the frequency, at which the maximal amplitude occurs, is plotted as a function of probe power. The image is qualitatively similar to figure 4.6. Again ω_{max} is higher for the sweep up measurement compared to the sweep down measurement for high probe powers.

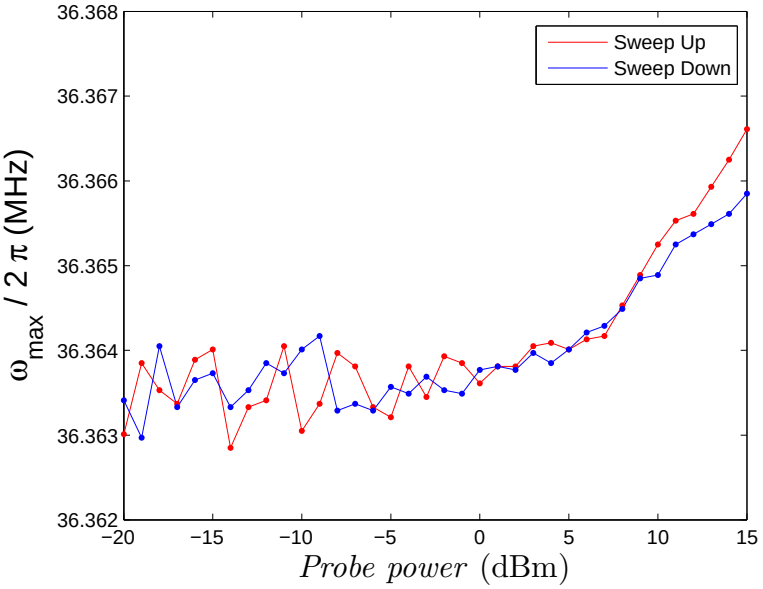

Figure 4.9: Frequency at which the maximal amplitude occurs for the different probe powers and a fixed pump power of 17 dBm. When the amplitude response becomes more duffing the difference between the bifurcation frequencies becomes larger. As a result the red and blue curve split.

The value of α is determined in exactly the same way as in the previous section. The frequency, at which the maximum amplitude occurs, is plotted as a function of the mechanical amplitude squared and fitted with a

straight line. The slope of the fit is set equal to $\frac{3}{8}\frac{\alpha}{m\omega_0}$, which yields $\alpha = 3.2 \cdot 10^{17}\ kg/m^2s^2$

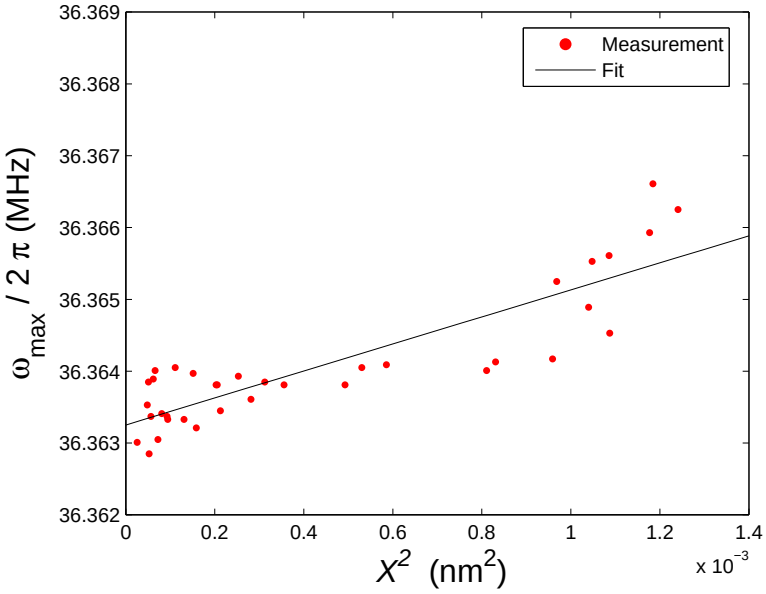

Figure 4.10: Frequency at which the maximal amplitude occurs as a function of mechanical amplitude squared for the different probe powers of the upward sweep. The pump power is fixed at 17 dBm. A linear fit is made through the measurements in accordance with equation (2.39). The slope is set equal to $\frac{3}{8}\frac{\alpha}{m\omega_0}$. This gives $3.2 \cdot 10^{17}\ kg/m^2s^2$ for the value of α.

5 Conclusion

In this research a multilayer graphene resonator was coupled to a superconducting microwave cavity. The mechanical resonator was driven by adding a RF signal and a DC voltage to the feedline. The reflection from the cavity was measured.

The mechanical repsonse of the multilayer graphene resonator could be altered by changing the pump or probe power. Low pump and probe powers gave a Lorentzian shape and high pump and probe powers gave a duffing shape as was predicted by the theory.

Further the hysteresis in the duffing regime due to the difference in bifurcation frequency was observed. The sweep up measurements had higher amplitudes and higher bifurcation frequencies than the sweep down measurements. This was also predicted by the theory.

Also in this research the effect of backaction on the quality factor and the nonlinear term in the restoring force[5] of the oscillator was investigated. The lower pump power of 14 dBm corresponds with less backaction and gave a quality factor of 148899 and an α of $3.3 \cdot 10^{16}\ kg/m^2s^2$. The higher pump power of 17 dBm yielded a quality factor of 62769 and $3.2 \cdot 10^{17}\ kg/m^2s^2$ for the value of α. The conclusion is that backaction not only decreases the quality factor, but also causes an increase in the value of α.

[5]See equation (2.15)

References

[1] Geim, A.K., Novoselov, K.S., The rise of graphene,*Nature Materials* **6** 183 (2007)

[2] Stormer et al, Ultrahigh electron mobility in suspended graphene, *Solid State Communications* **146** (2008)

[3] Sood, K. et al, Monitoring dopants by Raman scattering in an electrochemically top gated graphene transistor, *Nature Technology* **3** 210-215 (2008)

[4] Hone et al, Measurement of the Elastic Properties and Intrinsic Strength of Monolayer Graphene, *Science* **321** 5887 (2008)

[5] Geim, A.K., Graphene: Status and Prospects, *Science* **19** 324 (2009)

[6] Barton, R.A. et al, High, size-dependent quality factor in an array of graphene mechanical resonators, *Nano Letters* **11**, 1232-1236 (2011)

[7] Dai, M.D., Kim, C.W., Eom, K., Nonlinear vibration behavior of graphene resonators and their application in sensitive mass detection, *Nanoscale Research Letters*, **7** 499 (2012)

[8] Chen, C. et al. Performance of monolayer graphene nanomechanical resonators with electrical readout, *Nat Nano* **4**, 861-867 (2009)

[9] Aspelmeyer, M., Kippenberg, T.J., Marquardt, F., *Cavity Optomechanics*, (2013)

[10] Kippenberg, T.J., Vahala, K.J., Cavity Optomechanics Back-Action at the Mesoscale,*Phys. Rev.* **321** 1172-1176 (2008)

[11] Teufel, J.D., Sideband cooling of micromechanical motion to the quantum ground state, *Nature* **475** 359-363 (2011)

[12] Palomaki, T.A., Teufel, J.D., Simmonds, R.W., Lehnert, K.W., Entangling mechanical motion with microwave fields, *Science* **342** 710-713 (2013)

[13] Lehnert, K.W. et al, Nanomechanical motion measured with an imprecision below that at the standard quantum limit, *Nature Nanotechnology* **4** 820-823 (2009)

[14] Steele et al, Optomechanical coupling between a graphene mechanical resonator and a superconducting microwave cavity, (2014)

[15] Eichler, A. et al, Nonlinear damping in mechanical resonators made from carbon nanotubes and graphene, *Nature Technology* **6** 339-342 (2011)

[16] Elert, G.,Measuring Chaos, *The Chaos Hypertextbook*, (2007)

[17] Lifshitz, R., Cross, M.C., Nonlinear dynamics of nanomechanical and micromechanical resonators, *Review of Nonlinear Dynamics and Complexity* ***1*** (2008)

[18] Weis, S. et al, Optomechanically Induced Transparency, *Science* **10** 330 (2010)

[19] Pozar, D.M., *Microwave Engineering*, (2012)

Appendices

Appendix A

The term β proportional to x^2 in the restoring force and the term μ proportional to $x\dot{x}$ in the dampling force only rescale the values of α and η (see equation (2.14) and (2.15)). The equation of motion with the additional terms is given by eqaution (A.1).

$$m\ddot{x} = \underbrace{-kx - \beta x^2 - \alpha x^3}_{\text{restoring force}} \quad \underbrace{-l\dot{x} - \mu x\dot{x} - \eta x^2\dot{x}}_{\text{damping force}} \quad + \quad \underbrace{Bcos(\omega t)}_{\text{driving force}} \tag{A.1}$$

The following substitions are made in order to make the variables dimensionless.

$$\tilde{x} = x\sqrt{\frac{\alpha}{m\omega_0^2}} \qquad and \qquad \tilde{t} = \omega_0 t \tag{A.2}$$

After the substitutions and dividing by $m\omega_0^2\sqrt{\frac{m\omega_0^2}{\alpha}}$ the dimensionless equation of motion is obtained.

$$\ddot{\tilde{x}} + \tilde{x} + \tilde{\beta}\tilde{x}^2 + \tilde{x}^3 + Q^{-1}\dot{\tilde{x}} + \tilde{\mu}\tilde{x}\dot{\tilde{x}} + \tilde{\eta}\tilde{x}^2\dot{\tilde{x}} = Gcos(\tilde{\omega}\tilde{t}) \tag{A.3}$$

The relation of the dimensionless parameters with the physical ones are apart from equation (A.2) given in equation (A.4).

$$\tilde{\beta} = \frac{\beta}{\sqrt{m\omega_0^2\alpha}} \qquad Q^{-1} = \frac{l}{m\omega_0} \qquad \tilde{\mu} = \frac{\mu}{\sqrt{m\alpha}} \qquad \tilde{\eta} = \frac{\eta\omega_0}{\alpha} \qquad G = \frac{B}{\omega_0^3}\sqrt{\frac{\alpha}{m^3}} \qquad \tilde{\omega} = \frac{\omega}{\omega_0} \tag{A.4}$$

Again the method of multiple scales is used to approximate the solution of equation (A.3). Define ϵ again as the reciprocal of the quality factor ($\epsilon = Q^{-1}$) and make two transformations: $G = \epsilon^{3/2}g$ and $\tilde{\omega} = 1 + \epsilon\Omega$. The new form of the dimensionless equation of motion is given by equation (A.5).

$$\ddot{\tilde{x}} + \tilde{x} + \tilde{\beta}\tilde{x}^2 + \tilde{x}^3 + \epsilon\dot{\tilde{x}} + \tilde{\mu}\tilde{x}\dot{\tilde{x}} + \tilde{\eta}\tilde{x}^2\dot{\tilde{x}} = \epsilon^{3/2}g\cos\left[(1+\epsilon\Omega)\tilde{t}\right] \tag{A.5}$$

The solution of equation (A.5) can be expressed by the following expansion.

$$\tilde{x}(\tilde{t}) = \sqrt{\epsilon}x_0(\tilde{t}) + \epsilon x_{1/2}(\tilde{t}) + \epsilon^{3/2}x_1(\tilde{t}) + O(\epsilon^2) \tag{A.6}$$

Note that there are now also terms of order ϵ. The definitions of the slow and fast time are: $T_0 = \tilde{t}$ and $T_1 = \epsilon\tilde{t}$. The first and second derivative of the dimensionless position are now calculated. Terms of order ϵ^2 and higher are neglected.

$$\frac{d\tilde{x}}{d\tilde{t}} = \sqrt{\epsilon}\frac{\partial x_0}{\partial T_0} + \epsilon\frac{\partial x_{1/2}}{\partial T_0} + \epsilon^{3/2}\left[\frac{\partial x_1}{\partial T_0} + \frac{\partial x_0}{\partial T_1}\right] + O(\epsilon^2) \tag{A.7a}$$

$$\frac{d^2\tilde{x}}{d\tilde{t}^2} = \sqrt{\epsilon}\frac{\partial^2 x_0}{\partial T_0^2} + \epsilon\frac{\partial^2 x_{1/2}}{\partial T_0^2} + \epsilon^{3/2}\left[\frac{\partial^2 x_1}{\partial T_0^2} + 2\frac{\partial^2 x_0}{\partial T_0 \partial T_1}\right] + O(\epsilon^2) \tag{A.7b}$$

The expansions of the derivatives are now inserted into equation (A.5).

$$\sqrt{\epsilon}\frac{\partial^2 x_0}{\partial T_0^2} + \epsilon\frac{\partial^2 x_{1/2}}{\partial T_0^2} + \epsilon^{3/2}\frac{\partial^2 x_1}{\partial T_0^2} + 2\epsilon^{3/2}\frac{\partial^2 x_0}{\partial T_0 T_1} + \sqrt{\epsilon}x_0 + \epsilon x_{1/2} + \epsilon^{3/2}x_1 + \tilde{\beta}\left(\sqrt{\epsilon}x_0 + \epsilon x_{1/2}\right. \tag{A.8}$$

$$\left.+\epsilon^{3/2}x_1\right)^2 + \left(\sqrt{\epsilon}x_0 + \epsilon x_{1/2} + \epsilon^{3/2}x_1\right)^3 + \epsilon\left(\sqrt{\epsilon}\frac{\partial x_0}{\partial T_0} + \epsilon\frac{\partial x_{1/2}}{\partial T_0} + \epsilon^{3/2}\frac{\partial x_1}{\partial T_0} + \epsilon^{3/2}\frac{\partial x_0}{\partial T_1}\right) + \tilde{\mu}\left(\sqrt{\epsilon}x_0\right. \tag{A.9}$$

$$\left.+\epsilon x_{1/2} + \epsilon^{3/2}x_1\right)\left(\sqrt{\epsilon}\frac{\partial x_0}{\partial T_0} + \epsilon\frac{\partial x_{1/2}}{\partial T_0} + \epsilon^{3/2}\frac{\partial x_1}{\partial T_0} + \epsilon^{3/2}\frac{\partial x_0}{\partial T_1}\right) + \tilde{\eta}\left(\sqrt{\epsilon}x_0 + \epsilon x_{1/2} + \right. \tag{A.10}$$

$$\left.\epsilon^{3/2}x_1\right)^2\left(\sqrt{\epsilon}\frac{\partial x_0}{\partial T_0} + \epsilon\frac{\partial x_{1/2}}{\partial T_0} + \epsilon^{3/2}\frac{\partial x_1}{\partial T_0} + \epsilon^{3/2}\frac{\partial x_0}{\partial T_1}\right) = \epsilon^{3/2}gcos(T_0 + T_1\Omega) \tag{A.11}$$

Comparing coefficients for $\sqrt{\epsilon}$, ϵ and $\epsilon^{3/2}$ gives:

$$\frac{\partial^2 x_0}{\partial T_0^2} + x_0 = 0 \tag{A.12a}$$

$$\frac{\partial^2 x_{1/2}}{\partial T_0^2} + x_{1/2} + \tilde{\beta} x_0 + \tilde{\mu} x_0 \frac{\partial x_0}{\partial T_0} = 0 \tag{A.12b}$$

$$\frac{\partial^2 x_1}{\partial T_0^2} + 2\frac{\partial^2 x_0}{\partial T_0 \partial T_1} + x_1 + 2\tilde{\beta} x_0 x_{1/2} + x_0^3 + \frac{\partial x_0}{T_0} + \tilde{\mu} x_0 \frac{\partial x_{1/2}}{\partial T_0} + \tilde{\mu} x_{1/2} \frac{\partial x_0}{\partial T_0} + \tilde{\eta} x_0^2 \frac{\partial x_0}{\partial T_0} = g\cos(T_0 + T_1\Omega) \tag{A.12c}$$

The general solution of equation (A.12a) may be written as: $x_0 = \frac{1}{2}A(T_1)e^{jT_0} + c.c.$ .With the help of this solution equation (A.12b) is rewritten.

$$\frac{\partial^2 x_{1/2}}{\partial T_0^2} + x_{1/2} = -\frac{\tilde{\beta}}{2}|A|^2 - \frac{1}{4}\left[(\tilde{\beta} + \tilde{\mu} j)A^2 e^{2jT_0} + c.c.\right] \tag{A.13}$$

Equation (A.13) contains no secular terms and can be solved directly.

$$x_{1/2} = -\frac{\tilde{\beta}}{2}|A|^2 + \frac{1}{12}\left[(\tilde{\beta} + \tilde{\mu} j)A^2 e^{2jT_0} + c.c.\right] \tag{A.14}$$

The expressions of x_0 and $x_{1/2}$ can be used to rewrite equation (A.12c).

$$\frac{\partial^2 x_1}{\partial T_0^2} + x_1 = -\left[j\left(\frac{dA}{dT_1} + \frac{1}{2}A + \frac{1}{8}\left(\tilde{\eta} - \tilde{\mu}\tilde{\beta}\right)A^2 A^*\right) + \frac{3}{8}\left(1 - \frac{10}{9}\tilde{\beta}^2 - \frac{1}{9}\tilde{\mu}^2\right)A^2 A^* - \frac{g}{2}e^{jT_1\Omega}\right]e^{jT_0} + \text{nonsecular terms} \tag{A.15}$$

Setting the secular term to zero and rearranging the equation gives:

$$\frac{dA}{dT_1} = -\frac{1}{2}A - \frac{1}{8}\left(\tilde{\eta} - \tilde{\mu}\tilde{\beta}\right)A^2 A^* + \frac{3}{8}j\left(1 - \frac{10}{9}\tilde{\beta}^2 - \frac{1}{9}\tilde{\mu}^2\right)A^2 A^* - \frac{g}{2}je^{jT_1\Omega} \tag{A.16}$$

The form of equation (A.16) equation is similar to equation (2.32). We introduce an effective $\tilde{\eta}$ and $\tilde{\alpha}$.

$$\frac{dA}{dT_1} = -\frac{1}{2}A - \frac{1}{8}\tilde{\eta}_{eff}A^2 A^* + \frac{3}{8}j\tilde{\alpha}_{eff}A^2 A^* - \frac{g}{2}je^{jT_1\Omega} \tag{A.17}$$

Where:

$$\tilde{\eta}_{eff} = \tilde{\eta} - \tilde{\mu}\tilde{\beta} \tag{A.18a}$$

$$\tilde{\alpha}_{eff} = 1 - \frac{10}{9}\tilde{\beta}^2 - \frac{1}{9}\tilde{\mu}^2 \tag{A.18b}$$

The amplitude and phase equations ((2.35a) and (2.35b)) still apply except that $\tilde{\eta}$ is now replaced with $\tilde{\eta}_{eff}$ and $\tilde{\alpha}$ is replaced with $\tilde{\alpha}_{eff}$. We conclude that the term β proportional to x^2 in the restoring force and the term μ proportional to $x\dot{x}$ in the dampling force only rescale the values of α and η.

Appendix B

The discussion and derivations of the transmission line are based on [19]. Photons are coupled in and out of the cavity with the help of a transmission line. A transmission line is ussually long comparable to the wavelenght of the light. Voltages and current vary in magnitude and phase over its length. A model of a

ModelTransmissionLine.png

Figure B.1: Model for a transmission line.

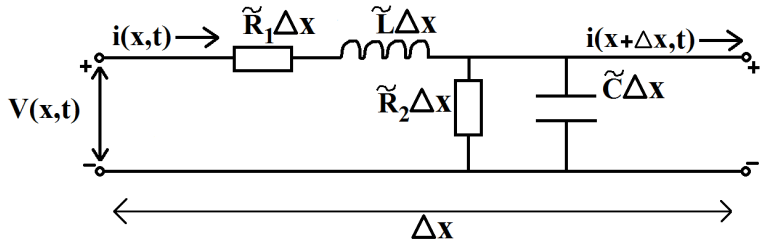

Figure B.2: A small lenght Δx of a transmission line.

transmission line is shown in figure B.1. The resistance R_1 is due to the finite conductivity of the conductors, the solenoid L represents the self-inductance of the two conductors, the resistance R_2 stands for dielectric losses between the conductors and the capacitance C is due to the close proximity of the two conductors. A slice of the transmission line with width Δx is shown in figure B.2. Where $\tilde{R}$ represents the resistance per unit length, $\tilde{L}$ the inductance per unit length and $\tilde{C}$ the capacitance per unit length. Kirchhoff's law for voltage and current is applied to figure B.2.

$$v(x,t) - \tilde{R}_1 \Delta x i(x,t) - \tilde{L}\Delta x \frac{\partial i}{\partial t} - v(x+\Delta x, t) = 0 \tag{B.1a}$$

$$i(x,t) - \tilde{G}_2 \Delta x v(x,t) - \tilde{C}\Delta x \frac{\partial v}{\partial t} - i(x+\Delta x.t) = 0 \tag{B.1b}$$

Note that $\tilde{G}_2$ is the conductance per unit lenght $(1/\tilde{R}_2)$. Divide both equations by Δx and take the limit $\Delta x \to 0$.

$$\frac{\partial v}{\partial x} = -\tilde{R}_1 i(x,t) - \tilde{L}\frac{\partial i}{\partial t} \tag{B.2a}$$

$$\frac{\partial i}{\partial t} = -\tilde{G}_2 v(x,t) - \tilde{C}\frac{\partial v}{\partial t} \tag{B.2b}$$

The Fourier transform of both equations is taken.

$$\frac{\partial V}{\partial x} = -(\tilde{R}_1 + j\omega\tilde{L})I(x,\omega) \tag{B.3a}$$

$$\frac{\partial I}{\partial x} = -(\tilde{G}_2 + j\omega\tilde{C})V(x,\omega) \tag{B.3b}$$

Combining both equations gives:

$$\frac{\partial^2 V}{\partial x^2} - \gamma^2 V(x,\omega) = 0 \tag{B.4a}$$

$$\frac{\partial^2 I}{\partial x^2} - \gamma^2 I(x,\omega) = 0 \tag{B.4b}$$

Where:

$$\gamma = \alpha + j\beta = \sqrt{(\tilde{R}_1 + j\omega\tilde{L})(\tilde{G}_2 + j\omega\tilde{C})} \tag{B.5}$$

The general solutions of the equations (B.4a) and (B.4b) are:

$$V(x,\omega) = V_0^+ e^{-\gamma x} + V_0^- e^{\gamma x} \tag{B.6a}$$

$$I(x,\omega) = I_0^+ e^{-\gamma x} + I_0^- e^{\gamma x} \tag{B.6b}$$

Here $e^{-\gamma x}$ is the wave propagating in the positive x-direction and $e^{\gamma x}$ is the wave propagating in the negative x-direction. Now combine equations (B.3a) and (B.6a) or equations (B.3b) and (B.6b) to get:

$$Z_0 = \frac{V_0^+}{V_0^+} = -\frac{V_0^-}{I_0^-} = \frac{\tilde{R}_1 + j\omega\tilde{L}}{\gamma} = \sqrt{\frac{\tilde{R}_1 + j\omega\tilde{L}}{\tilde{G}_2 + j\omega\tilde{C}}} \tag{B.7}$$

If the transmission line is in the superconducting regime we can set $\tilde{R}_1 = 0$ and $\tilde{R}_2 = \infty$. This gives:

$$Z_0 = \sqrt{\frac{\tilde{L}}{\tilde{C}}} \tag{B.8}$$

In the superconducting regime the impedance of the transmission line solely depends on the self-inductance and the capacitance per unit lenght.

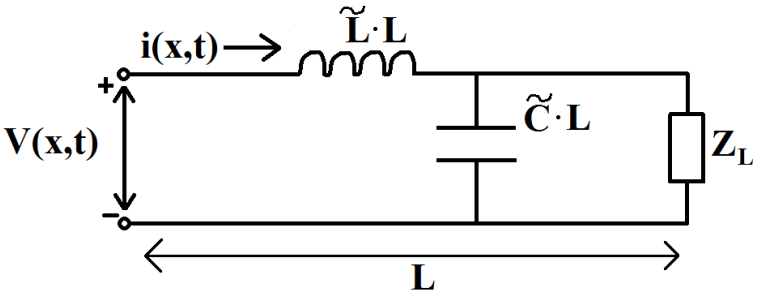

Figure B.3: Model for a lossless transmission line with a load. L is the total lenght of the transmission line.

Now the influence of the attachment of an arbritary load to the transmission line is discussed. In figure B.3 the transmission line with the attachted load is shown. Assume that the transmission line is in the superconducting regime. Expanding equation (B.5) and setting R_1 and G_2 to zero yields:

$$\gamma = j\omega\sqrt{\tilde{L}\tilde{C}} \tag{B.9}$$

And thus:

$$\beta = \omega\sqrt{\tilde{L}\tilde{C}} \tag{B.10}$$

The solutions for the voltage and current in the frequency domain are now adjusted to the superconducting regime (equations (B.6a) and (B.6b)).

$$V(x,\omega) = V_0^+ e^{-\beta x} + V_0^- e^{\beta x} \tag{B.11a}$$

$$I(x,\omega) = \frac{V_0^+}{Z_0} e^{-\beta x} - \frac{V_0^-}{Z_0} e^{\beta x} \tag{B.11b}$$

Assume that an incident wave of the form $V_0^+ e^{-\beta x}$ is generated from the source. We identify $V_0^- e^{\beta x}$ as the relected wave. The load is located at $x = 0$. Z_L must be equal to the voltage divided by the current at the location of the load.

$$Z_L = \frac{V_0^+ + V_0^-}{V_0^+ - V_0^-} Z_0 \tag{B.12}$$

Equation (B.12) is rewritten to get an explicit expression for the amplitude of the reflected wave.

$$V_0^- = V_0^+ \frac{Z_L - Z_0}{Z_L + Z_0} \tag{B.13}$$

The amplitude of the reflected wave is often divided by the amplitude of the incident wave.

$$\Gamma = \frac{V_0^-}{V_0^+} = \frac{Z_L - Z_0}{Z_L + Z_0} \tag{B.14}$$

The voltage and current are now rewritten in terms of Γ.

$$V(x,\omega) = V_0^+ (e^{-\beta x} + \Gamma e^{\beta x}) \tag{B.15a}$$

$$I(x,\omega) = \frac{V_0^+}{Z_0} (e^{-\beta x} - \Gamma e^{\beta x}) \tag{B.15b}$$

The voltage and the current in the transmission line consist of a superposition of the incident and reflected wave. Also note that if the load is matched to the impedance of the transmission line Γ becomes zero. There is no reflected wave is this case. The reflection is maximal when $Z_L = \infty$ or when $Z_L = 0$. (When $Z_L = 0$,

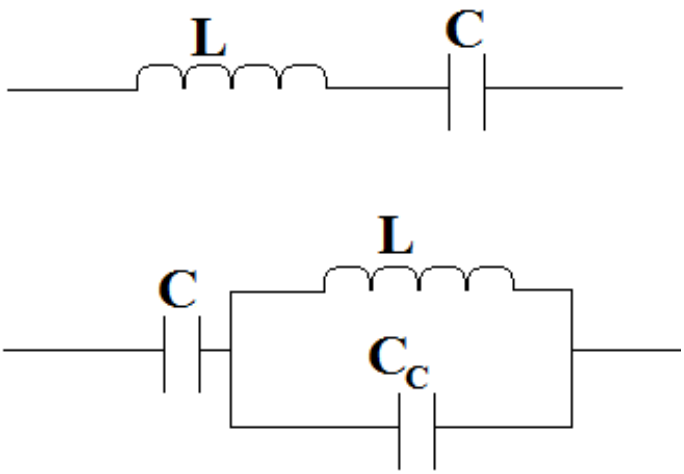

Figure B.4: Two circuits that are equivalent except for a scaling factor.

$\Gamma = -1$ which means there is a phase shift of 180°).

The series connection of the inductance and the capacitor in the transmissionline (figure B.3) has a scaled equivalent of a capacitor in series with a parallel circuit of an inductance and a capacitor for frequencies near the resonance frequency.

Figure B.4 shows the two circuits. The impedance of the lowest of the two circuits displayed in figure B.4 is given by equation (B.16).

$$Z = \frac{1}{j\omega C} + \frac{j\omega L \cdot 1/j\omega C_c}{j\omega L + 1/j\omega C_c} \tag{B.16}$$

Equation (B.16) can be rewritten.

$$Z = \frac{1}{j\omega C} + j\omega L \left[\frac{1}{1 - \frac{\omega^2}{\omega_0^2}} \right] \tag{B.17}$$

In equation (B.17): $\omega_0 = 1/\sqrt{LC}$, the resonance frequency of the circuit. Assume that the the frequency of an incoming signal is near the resonance frequency: $\omega = \omega_0 + \delta$. Substituting this in equation (B.17) and neglecting the term of order δ^2 gives:

$$Z = \frac{1}{j\omega C} + \beta \cdot j\omega L \tag{B.18}$$

Where: $\beta = -\omega_0/2\delta$. Equation (B.18) is the impedance for a series connection of a capacitor and an inductance with a scaling factor β.

Appendix C

In this appendix the backaction on the cavity and mechanical resonator is discussed. The presence of the oscillator effects the internal dissipation rate when the oscillator is driven at the blue or red side band. The red side band is the frequency $\omega_c - \omega_m$ and the blue side band is the frequency $\omega_c + \omega_m$. Where ω_c is the cavity resonant frequency and ω_m the mechanical resonant frequency of the oscillator.

$$\kappa_0^{eff} = \kappa_0 \pm \frac{4g^2}{\gamma_m^{eff}} \tag{C.1}$$

Where:

$$g = G \cdot x_{zpf} \cdot \sqrt{n_d} \tag{C.2}$$

$$\gamma_m^{eff} = \gamma_m(1 \pm C) \tag{C.3}$$

And:

$$C = \frac{4g_0^2 n_d}{\gamma_m \kappa} \tag{C.4}$$

In equation (C.2) G is the pull in parameter, x_{zpf} is the zero point motion of the oscillatora and$\sqrt{n_d}$ is the number of drive photons. The plus sign in equation (C.1) corresponds with the red side band and the minus sign with the blue side band. Equations (2.52a) and (2.52b) are adjusted.

$$R = \frac{\langle \hat{a}_{out} \rangle}{\langle \hat{a}_{in} \rangle} = \frac{(\kappa_0^{eff} - \kappa_{ex})/2 - i\Delta}{(\kappa_0^{eff} + \kappa_{ex})/2 - i\Delta} \tag{C.5a}$$

$$\phi = \arctan\left(\frac{4\Delta\kappa_{ex}}{(\kappa_0^{eff})^2 - \kappa_{ex}^2 + 4\Delta^2}\right) \tag{C.5b}$$

The change of the internal dissipation rate effects the coupling efficiency.

$$\eta^{eff} = \frac{\kappa_{ex}}{\kappa_0^{eff} + \kappa_{ex}} \tag{C.6}$$

Appendix D

In section 4.3 the probe power was swept with a fixed pump power. The chosen pump powers were 14 dBm and 17 dBm. This part of the appendix explains why this decision was made.

The cavity is driven at the red side band frequency: $\omega_d = 2\pi \cdot 5.864187\ GHz$. The pump power is varied from 0 till 30 dBm and ω_p is swept. The signal is measured at all integers from 0 dBm to 30 dBm. Figure D.1 shows the amplitude of the signal as a function of probe power.

As the drive power goes up from 0 dBm the amplitude initially rises, but starts to decrease at powers higher than 15 dBm. This is caused by backaction and can be explained with the help of figure 2.6 and equations (C.1) and (C.6) in appendix C. The change in drive power changes the internal dissipation rate and this leads to a change in the coupling efficieny. The amplitude is maximal at critical coupling but decreases when the coupling is changed to the undercoupling or overcoupling regime. This can be seen in the left image of figure 2.6. Initially the amplitude increases with increasing drive power, but when the η starts to become smaller the cavity becomes undercoupled and the amplitude decreases (see the right image in figure 2.6).
When the amplitude of the signal is too small the signal to noise ratio is bad. This means that pump powers should be chosen where the amplitude of the signal is large. We want one pump power that gives a good signal to noise ratio but where backaction is *not* significant and we want one pump power that gives a good signal to noise ratio and where backaction *is* significant. Based on the above the choice of the two pump powers of 14 dBm and 17 dBm are justified.

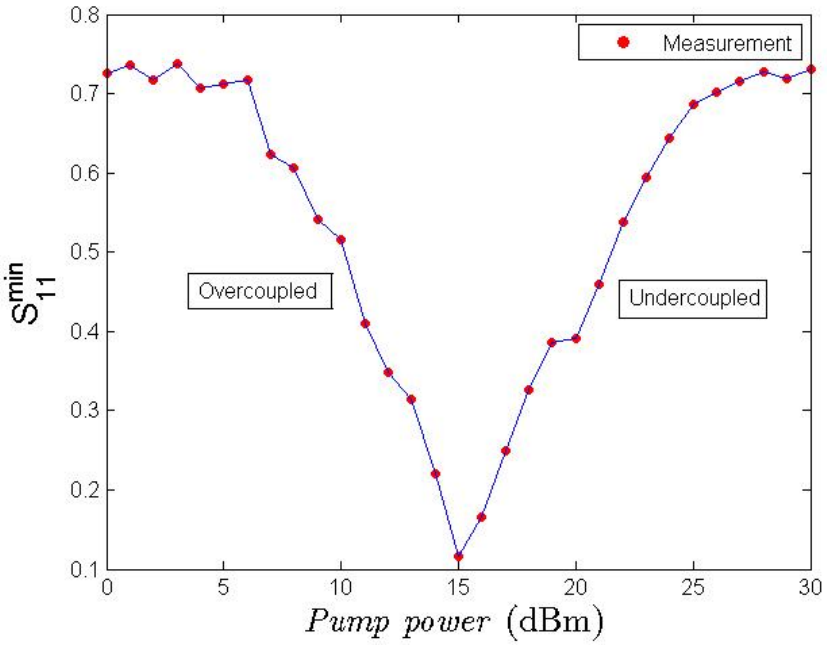

Figure D.1: The cavity is driven at the red side band frequency and the pump power is varied. The change in pump power influences the coupling efficiency through backaction. When the cavity becomes undercoupled the amplitude of the signal starts to decrease for increasing pump powers. This figure can be compared with the right image of figure 2.6.